JOURNAL OF GEOPHYSICAL RESEARCH, VOL. 113, E05007, doi:10.1029/2007JE002997, 2008

Formation and distribution of benzene on Titan

V. Vuitton,[1] R. V. Yelle,[1] and J. Cui[1]

Received 29 August 2007; revised 17 December 2007; accepted 30 January 2008; published 30 May 2008.

[1] We present a study of the formation and distribution of benzene (C_6H_6) on Titan. Analysis of the Cassini Mass Spectrometer (INMS) measurements of benzene densities on 12 Titan passes shows that the benzene signal exhibits an unusual time dependence, peaking ~20 s after closest approach, rather than at closest approach. We show that this behavior can be explained by recombination of phenyl radicals (C_6H_5) with H atoms on the walls of the instrument and that the measured signal is a combination of (1) C_6H_6 from the atmosphere and (2) C_6H_6 formed within the instrument. In parallel, we investigate Titan benzene chemistry with a set of photochemical models. A model for the ionosphere predicts that the globally averaged production rate of benzene by ion-molecule reactions is $\sim 10^7$ cm^{-2} s^{-1}, of the same order of magnitude as the production rate by neutral reactions of $\sim 4 \times 10^6$ cm^{-2} s^{-1}. We show that benzene is quickly photolyzed in the thermosphere, and that C_6H_5 radicals, the main photodissociation products, are ~3 times as abundant as benzene. This result is consistent with the phenyl/benzene ratio required to match the INMS observations. Loss of benzene occurs primarily through reaction of phenyl with other radicals, leading to the formation of complex aromatic species. These species, along with benzene, diffuse downward, eventually condensing near the tropopause. We find a total production rate of solid aromatics of $\sim 10^{-15}$ g cm^{-2} s^{-1}, corresponding to an accumulated surface layer of ~3 m.

Citation: Vuitton, V., R. V. Yelle, and J. Cui (2008), Formation and distribution of benzene on Titan, *J. Geophys. Res.*, *113*, E05007, doi:10.1029/2007JE002997.

1. Introduction

[2] One of the more surprising results from the Cassini mission is the existence of remarkably complex molecules in the upper atmosphere of Titan [*Vuitton et al.*, 2006a; *Waite et al.*, 2007]. Although the existence of a robust chemistry on Titan was established by results from the Voyager mission [*Hunten et al.*, 1984], subsequent investigations tended to focus on the chemistry of the stratosphere rather than the thermosphere and ionosphere. For example, the seminal study by *Yung et al.* [1984], which served as a model for all subsequent photochemical models, considered the ionosphere as only a source of N atoms. The synthesis of complex molecules in the *Yung et al.* [1984] and subsequent models occurs primarily (sequentially) in the stratosphere. Some later work attempted to include coupling between the chemistry of the ionosphere and neutral atmosphere, but only in a simplified way and without the benefit of strong observational constraints [*Banaszkiewicz et al.*, 2000; *Wilson and Atreya*, 2004].

[3] It came as a surprise then, if not a shock, that Titan's upper thermosphere and ionosphere contained some very heavy molecules [*Vuitton et al.*, 2006a; *Waite et al.*, 2007]. The general rule in planetary atmospheres is that lighter species become more abundant at high altitudes because of diffusive separation and photo- and electron-dissociation processes, which operate primarily in the upper atmosphere. Titan goes against this trend with ions as heavy as several hundred amu [*Coates et al.*, 2007] and neutrals up to 91 amu [*Vuitton et al.*, 2007]. It is likely that even heavier neutrals are present but are beyond the mass range of Cassini instruments.

[4] The most abundant heavy molecule in Titan's thermosphere is the aromatic ring benzene (C_6H_6) [*Waite et al.*, 2005]. The first evidence for the presence of benzene in the atmosphere of Titan was found with the Infrared Space Observatory (ISO). A column density of 2.4×10^{15} cm^2 between 0.2 and 20 mbar and a mole fraction of 6.1×10^{-10} at 110 km averaged over all latitudes was retrieved [*Coustenis et al.*, 2003]. The Composite InfraRed Spectrometer (CIRS) onboard Cassini recently provided a firm detection of benzene in Titan's atmosphere and discovered strong benzene latitude variations in the stratosphere, with an increase of about an order of magnitude from south to north, reaching a maximum abundance of about 3.5×10^{-9} around 70°N [*Coustenis et al.*, 2007]. Limb scans reveal that the mixing ratio profile is mainly constant with altitude from 168 to 307 km at 80°N [*Vinatier et al.*, 2007]. These mid-IR observations are not sensitive to the high altitude benzene discovered by the INMS. Solid benzene has been tentatively identified on the surface by the Gas Chromatograph Mass Spectrometer (GCMS) [*Niemann et al.*, 2005]. Upon the impact of the Huygens probe, the GCMS inlet line heater

[1]Lunar and Planetary Laboratory, University of Arizona, Tucson, Arizona, USA.

0148-0227/08/2007JE002997$09.00

warmed the Titan surface, leading to the evaporation of liquid/solid materials and rendering their detection possible. The Visual Infrared Mapping Spectrometer (VIMS) onboard Cassini also reported a tentative detection of solid benzene on the surface (R. N. Clark, manuscript in preparation, 2008). These observations suggest that a substantial quantity of benzene is either produced by heterogeneous chemistry on the surface or through gas-phase chemistry in the atmosphere followed by condensation.

[5] The abundance of benzene detected by the Ion Neutral Mass Spectrometer (INMS) on the Cassini spacecraft [*Waite et al.*, 2007] is far greater than found in the stratosphere and far greater than predicted by pre-Cassini models of the composition of the upper atmosphere. The data from the closed ionization source indicate a mole fraction of a few ppm at an altitude of 1000 km, whereas photochemical models predicted a mole fraction of a few ppb. This suggests that the source of benzene is in the upper atmosphere.

[6] In order to investigate the complex chemistry in Titan's thermosphere and ionosphere further and understand its larger role in chemical cycles on Titan we present here an in-depth study of the formation and distribution of benzene on Titan. In section 2 we describe the INMS observations and data reduction in more detail than presented previously. In section 3, we analyze the response of the INMS to a gas mixture containing benzene, phenyl (C_6H_5), methyl (CH_3), and H. We explain the signal at m/z = 77 and 78 by a combination of atmospheric C_6H_6 and recombination of C_6H_5 radicals with H atoms on the walls of the closed source and the signal at m/z = 92 with the recombination of C_6H_5 with CH_3 radicals. We demonstrate that the benzene and phenyl densities required to fit the data are consistent with the results of the photochemical models discussed in section 4. The models show that benzene is efficiently produced by ion chemistry in the upper atmosphere. However, benzene is quickly photolyzed and phenyl radicals, the main photodissociation products, are ~3 times as abundant as benzene in the upper atmosphere. Loss of benzene occurs primarily through reaction of phenyl with other radicals, producing more complex aromatic species. Section 5 discusses these results and section 6 presents some concluding thoughts.

2. Observations and Data Reduction

2.1. Identification of C_6H_6 and C_7H_8

[7] Benzene has been observed in all of Cassini's low-altitude passes through Titan's atmosphere [*Waite et al.*, 2007]. Here we consider only measurements obtained with the Closed Source Neutral (CSN) channel of the INMS. This operational mode utilizes an enhancement chamber in front of the mass spectrometer that concentrates atmospheric molecules resulting in higher sensitivity for inert molecules that do not react with chamber walls [*Waite et al.*, 2005]. Observations in the Open Source Neutral mode have lower sensitivity and have not resulted in detection of benzene.

[8] CSN spectra obtained at low altitudes show a clear signal in the m/z = 73–79 region that we interpret as evidence for C_6H_6. Figures 1a–1b show spectra from the inbound and outbound legs of T16. The spectra represent averages over the 960–980 km region. Also shown are models for the benzene spectrum based on the INMS calibration (J. Cui, manuscript in preparation, 2008). The fit is excellent, confirming the identification of benzene. The high quality of the match between models and observations implies that C_6H_6 is likely benzene rather than any of the other (numerous) isomers. Figures 2a–2f show the benzene cracking pattern from the INMS calibration and the cracking patterns from the NIST database for benzene (Figure 2b) and several other isomers of C_6H_6 (Figures 2c–2f). The NIST data for benzene is quite similar to the INMS calibration data but both differ markedly from the cracking patterns for other isomers. In particular the signal at m/z = 60–62 is strong in most isomers, but weaker in benzene and in the INMS observations of Titan. This, along with the fact that it is the most stable isomer, strongly suggests that the signal is due to benzene.

[9] The count rates at m/z = 78 in the outbound measurements are complicated by a time shift discussed below; however, the inbound data are organized quite well as a function of altitude. Figures 3a–3b show the density at m/z = 78 for T16 and T23. Here, and in the following analysis, we concentrate on data from T16 because this pass penetrated the deepest into Titan's atmosphere and the benzene signal is strongest. Also shown are simple diffusive equilibrium models for a species of mass 78 amu assuming a constant temperature determined from analysis of the N_2 density distribution [*Müller-Wodarg et al.*, 2008]. These simple models provide an excellent fit to the data implying that the measured signal is due to an atmospheric species with a mass close to 78 amu. The benzene density distribution should only reflect the scale height for a mass of 78 amu if benzene is close to diffusive equilibrium. Analysis of INMS argon measurements indicates that the homopause on Titan is near 800 km [*Yelle et al.*, 2008] and that molecular diffusion should dominate over eddy mixing at the altitudes under consideration here. For the benzene distribution to be in diffusive equilibrium however, also requires that diffusion be faster than chemical production or loss processes. We will return to this in section 5.

[10] Aside from the benzene peaks at m/z = 62–63 and 73–79, there are no clear signatures at m/z > 60 for the inbound T16 spectrum shown in Figure 1a. However, the outbound T16 spectrum, shown in Figure 1b, has sizable peaks at m/z = 64–66 and m/z = 91–92. The first feature around m/z = 65 belongs to an unaccounted species. The signal around m/z = 91 is not much higher than the signal at the surrounding m/z but is statistically significant because of the much smaller associated error bars. The molecular weight suggests the chemical formula is C_7H_8 and the feature is well fit by an INMS calibration spectrum for toluene. We therefore consider this to be detection of toluene in the INMS closed source chamber. Structurally toluene is a benzene ring with a methyl radical substituted for an H atom, so given the detection of benzene, the presence of toluene is not surprising. In addition to the presence of the toluene signature, the outbound data has a much stronger benzene signature than the inbound data.

[11] Results from spectral analysis for the inbound data from INMS measurements to date are summarized in Table 1 along with geometrical data for each encounter. We do not include results from T17 or T20 because little neutral data

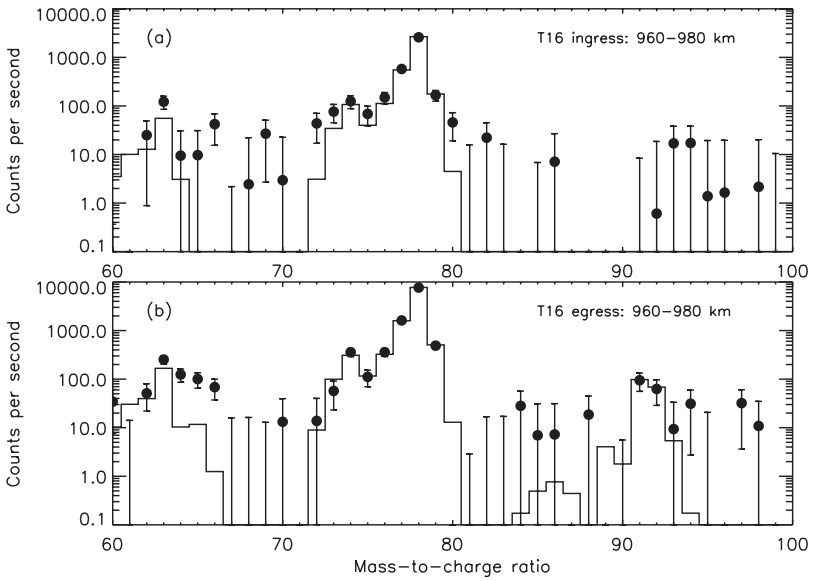

Figure 1. Data points represent a closed source neutral spectrum in the m/z = 60–99 region obtained during T16 and averaged over the 960–980 km range. The solid line is a model for the benzene and toluene spectra based on the INMS calibration. (a) Inbound leg. (b) Outbound leg.

were obtained. Included in Table 1 are the derived mole fractions for the lowest altitudes sampled (z1) and the predicted abundance at a constant pressure level of p0 = 1.45×10^{-5} Pa, which corresponds to an altitude of 1000 km at a latitude of 60°N. The latter values are calculated by fitting the altitude variation of the mole fraction for each pass to an exponential to predict the value at the altitude (z0) corresponding to p0. The mapping from altitude to pressure is based on the empirical model described by *Müller-Wodarg et al.* [2008].

[12] The derived mole fractions are roughly consistent with the preliminary results presented by *Waite et al.* [2007]. For reasons to be explained shortly, we believe that the derived densities do not represent the abundance of benzene in Titan's upper atmosphere, but rather a combination of the benzene and phenyl abundance that we will refer to as C_6H_x. To derive estimates of the benzene and phenyl mole fractions, it is necessary to examine the time behavior of the signals in more detail.

2.2. Time Variation of Signal

[13] Neutral species in Titan's upper atmosphere decrease rapidly with altitude and the temporal response of the INMS is extremely fast (tens of microseconds), implying that the measured signal should increase with time up to closest approach (C/A) and decrease thereafter. For example, Figure 4a shows that measurements of ethane (C_2H_6) at m/z = 30 during T16 have a maximum at C/A and are fairly symmetric about this time. The time dependence of the benzene and toluene signals, shown in Figures 4b–4d, is quite different. The signals peak ~20 s after C/A, rather than at C/A. Using the data shown in Figures 4b–4d, we calculate a time shift relative to C/A for m/z = 78, 77, and 92 of 27.0 ± 0.7, 22.5 ± 1.9, and 22.2 ± 6.6 s. The three time shifts are consistent within the uncertainties and the average shift is quite large.

[14] In principle, an asymmetry about C/A could be caused by large horizontal variations in the atmosphere. We consider this unlikely for two reasons. First, there is no evidence that the time shift varies from pass to pass, as would be expected if it were due to horizontal variations. This is shown in Figures 5a–5c where data from three Titan passes are plotted versus time from C/A. Despite the gaps in the measurements near C/A for T18 and T21 (due to other INMS observations being conducted at these times) the time behavior of all three encounters appear similar. The geometry of the 3 encounters is quite different however. T21, for example, has a C/A at 43.3° latitude and the sub-spacecraft latitude increases monotonically with time during the encounter [*Müller-Wodarg et al.*, 2008] while for T16 the maximum latitude of 85.5° is reached near C/A, as summarized in Table 1. Second, horizontal variations would have to be extremely large to cause the observed asymmetry. The data in Figures 5a–5c show that the INMS count rate in channel 78 is relatively constant from 0 to 50 s after C/A. The altitude changes by 12 km during that time (for T16), corresponding to a density decrease by a factor of 2, assuming that benzene has a diffusive equilibrium distribution. A constant signal implies that the horizontal variation in density must be of the same order over a latitudinal distance of 0.4°. This large a horizontal variation is unlikely and is inconsistent with the observed horizontal variations presented in Table 1. Thus we conclude that the anomalous time behavior of the signals is due to an internal process in the instrument rather than a property of the atmosphere.

[15] The low densities in Titan's upper atmosphere permit the development of relatively large densities of radicals. The photochemical calculations to be discussed in section 4 show that C_6H_5 is, in fact, more abundant than C_6H_6. This is a consequence of the extremely large C_6H_6 photolysis rate. Therefore we argue that the benzene and toluene are produced partly by radical recombination on the walls of the

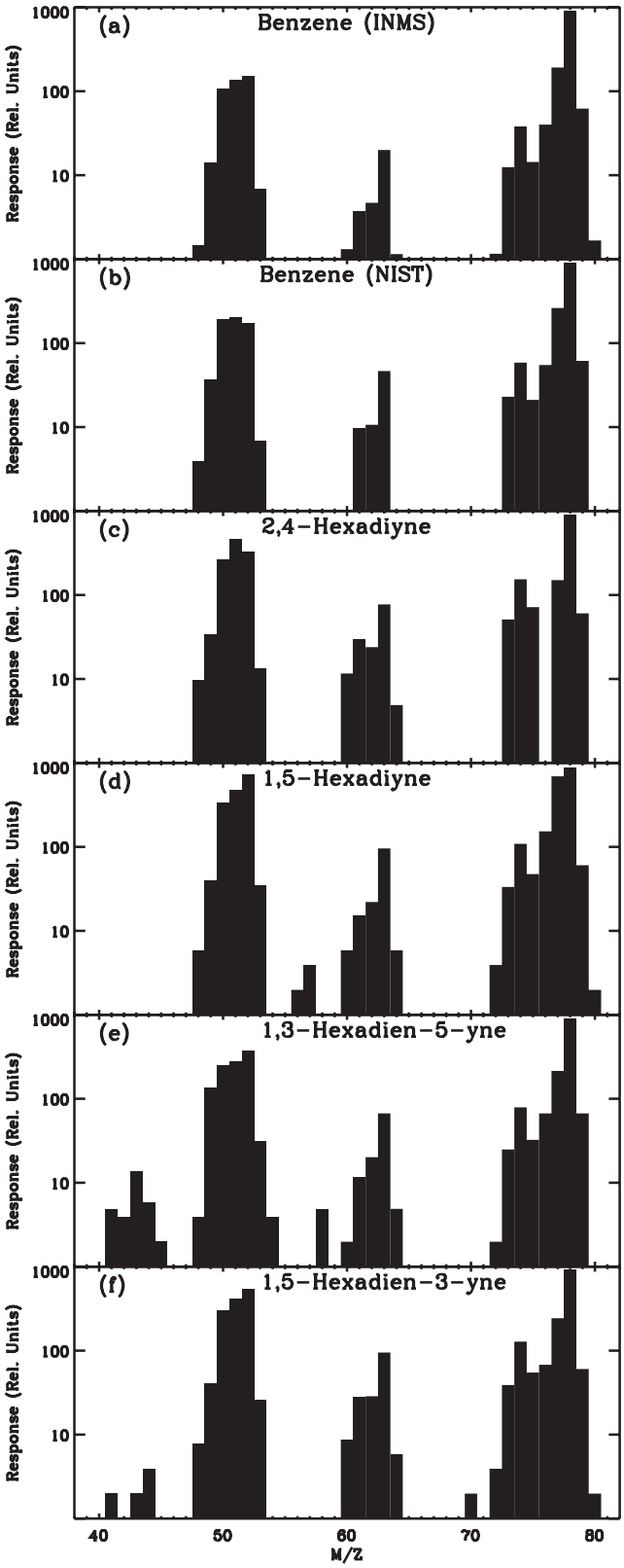

Figure 2. C_6H_6 isomers mass cracking patterns for an electron energy of 70 eV. (a) INMS calibration data for benzene. (b) NIST data for benzene. (c) NIST data for 2,4-Hexadiyne. (d) NIST data for 1,5-Hexadiyne. (e) NIST data for 1,3-Hexadien-5-yne. (f) NIST data for 1,5 Hexadien-3-yne.

INMS. This hypothesis is tested with a surface chemistry model in the next section.

3. Surface Chemistry Model

[16] The time delays in the C_6H_6 and C_7H_8 signals discussed in the previous section and the large abundance of H, CH_3, and C_6H_5 radicals discussed in section 4 suggest that these species are created by recombination of radicals adsorbed on the chamber walls. This hypothesis explains the time delay observed for these species because surface-diffusion limited reactions may require a significant amount of time. It explains the presence of both C_6H_6 and C_7H_8 because these are the products produced by reaction of the main radicals in the upper atmosphere. Methane should also be produced by reaction of CH_3 and H on the surface, but at a negligible rate near C/A because the density of atmospheric CH_4 is much greater than that of CH_3. The wall reaction hypothesis helps to reconcile the photochemical models with the measured C_6H_6 signal because, as discussed in the previous section, the phenyl abundance in the upper atmosphere is predicted to be larger than the benzene abundance. The INMS is really measuring the sum of benzene and phenyl and so the required production rate of benzene is significantly reduced compared with what is required if it were to be assumed that the signal were due to benzene alone.

[17] Recombination of radicals on chamber walls is a common phenomenon in spaceflight mass spectrometers and has on occasion been used to good advantage. For example, *Kasprzak et al.* [1980] determined the density of N in the Venusian upper atmosphere through analysis of the NO signal in the Pioneer Venus mass spectrometer under the assumption that NO was produced by desorption of NO, created by recombination of adsorbed N and O on the walls of the instrument. Other aspects of adsorption/desorption effects on spacecraft mass spectrometers are discussed in the work of *Hedin et al.* [1973]. Here we construct our own model for this process in order to interpret the INMS measurements in terms of atmospheric densities and the time constant for surface chemistry within the instrument.

[18] For simplicity of discussion we first consider formation of benzene. The time constants describing gas flow inside the instrument, equilibration of the walls and gas within the instrument, and the ionization and detection systems are all very small and we assume that the only significant time constant is for the rate of radical recombination on the walls of the closed-source enhancement chamber. In this case, the benzene density in the closed-source chamber is determined by the instantaneous balance between outflow from the entrance aperture to the chamber and the combination of the flow of benzene into the chamber from Titan atmosphere and desorption of benzene from the chamber walls. The desorption rate of benzene is assumed to be proportional to the triple product of phenyl surface density, H surface density, and the inverse of an empirical time constant. This time constant is determined by rate of diffusion over the surface of the chamber and the intrinsic reaction rate for adsorbed phenyl and H. To solve for the density of the adsorbed species in the chamber we

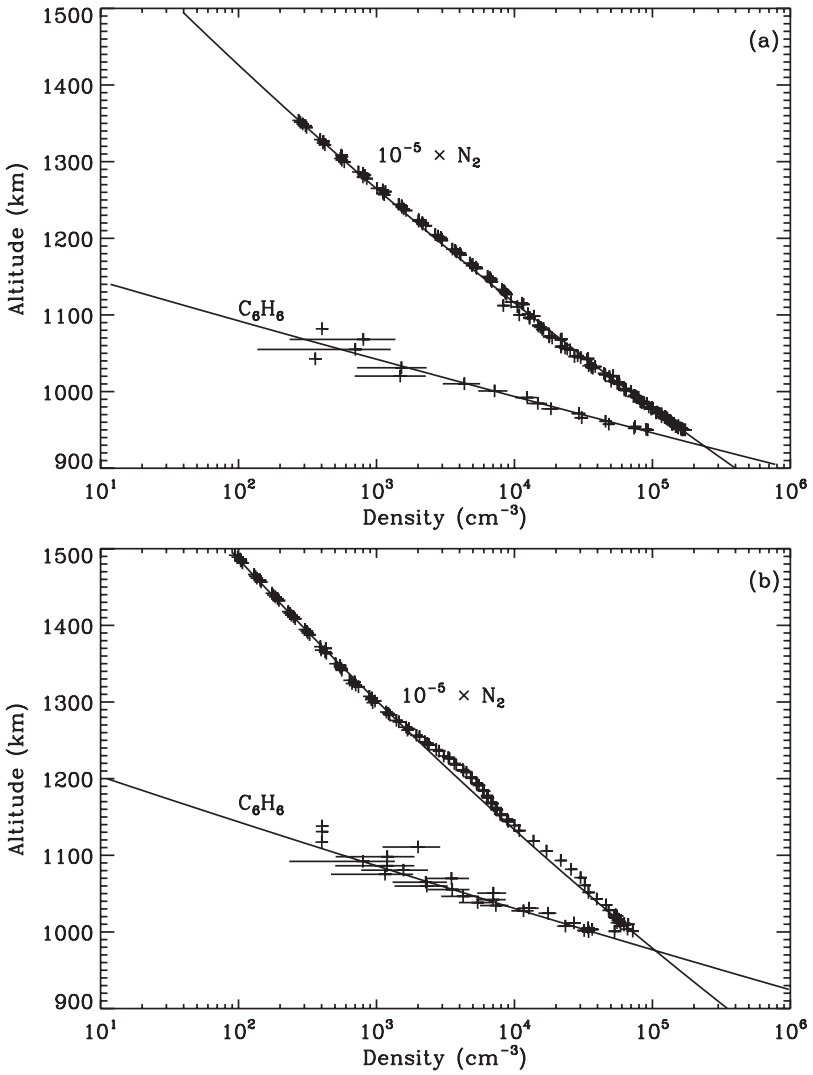

Figure 3. The variation of density with altitude for C_6H_6 (m/z = 78) and N_2 (m/z = 28, 14) measured by INMS. The solid lines indicate isothermal models to the altitude profile. (a) T16. Both C_6H_6 and N_2 are well fit by a temperature of 138 K. (b) T23. Both C_6H_6 and N_2 are well fit by a temperature of 154 K.

Table 1. Geometrical Parameters at C/A (Latitude, Longitude and Solar Zenith Angle) and C_6H_x Mole Fractions for 12 Titan Passes[a]

Pass	Latitude, deg	Longitude, deg	SZA, deg	z1, km	X1	z0, km	X0
T5	75.3	98.9	128.9	1038.6	2.2×10^{-7}	987.4	1.4×10^{-6}
T16	87.7	152.3	108.4	953.2	4.0×10^{-6}	968.8	2.2×10^{-6}
T18	76.6	12.6	92.9	972.3	3.8×10^{-6}	988.6	2.7×10^{-6}
T19	66.4	4.8	83.9	1021.4	9.6×10^{-7}	994.8	2.4×10^{-6}
T21	46.4	99.2	127.0	1020.8	8.9×10^{-7}	1004.4	1.5×10^{-6}
T23	33.9	1.0	54.8	1019.8	4.5×10^{-6}	1006.0	6.7×10^{-6}
T25	27.6	17.4	164.2	1004.7	1.0×10^{-6}	1006.3	9.9×10^{-7}
T26	25.7	1.8	155.4	991.9	3.5×10^{-6}	1006.3	2.8×10^{-6}
T27	39.0	0.4	146.3	1025.7	2.6×10^{-6}	1005.9	4.7×10^{-6}
T28	46.8	1.3	141.1	994.8	5.4×10^{-6}	1004.3	4.5×10^{-6}
T29	54.7	2.8	135.1	985.3	5.5×10^{-6}	1001.4	3.9×10^{-6}
T30	62.3	5.7	128.6	974.1	7.0×10^{-6}	997.2	4.2×10^{-6}

[a]X1 is the derived mole fraction for the lowest altitude sampled (z1) and X0 is the predicted abundance at a constant pressure level of p0 = 1.45×10^{-5} Pa, which corresponds to an altitude z0 of 1000 km at a latitude of 60°N. X1 and X0 represent a combination of the benzene and phenyl mole fractions (see section 3), they are not the real benzene atmospheric mole fraction. Uncertainties mostly come from calibration and are estimated to be about 20%.

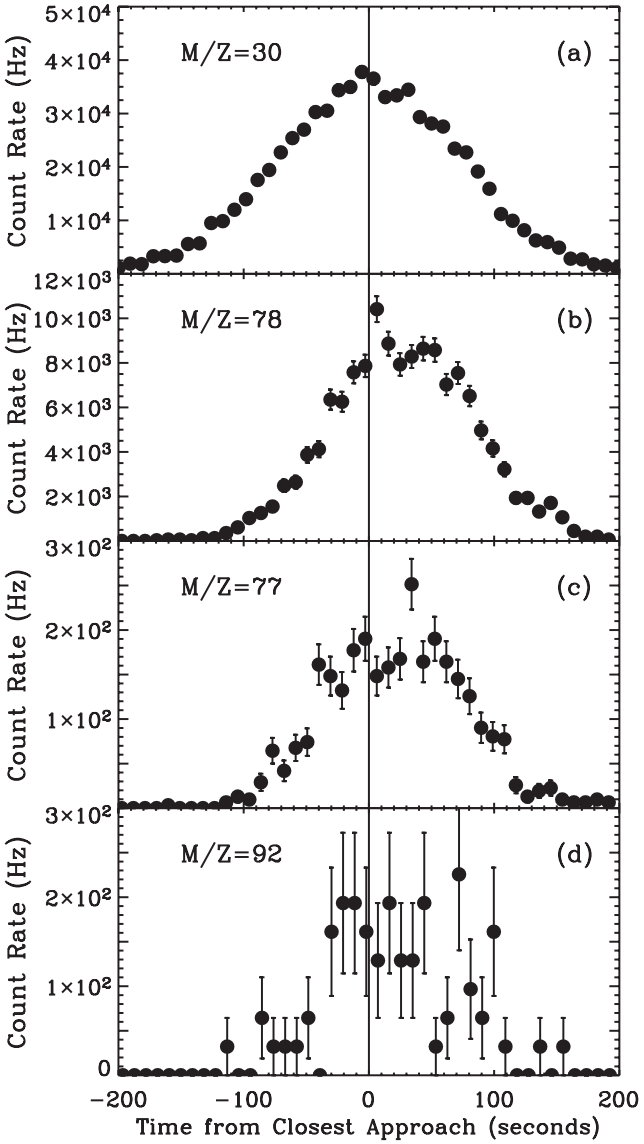

Figure 4. Time dependence of the signal from −200 to 200 s around closest approach for T16. (a) m/z = 30 (ethane). (b) m/z = 78 (benzene). (c) m/z = 77 (benzene). (d) m/z = 92 (toluene).

first consider the surface density on the chamber walls:

$$A_w \dot{M}_i = N_i^a(t) U_{sc} A_x - \Sigma \frac{1}{t_{ij}} \frac{M_i}{M_i^\circ} \frac{M_j}{M_j^\circ} \quad (1)$$

where M_i is the surface density of the adsorbed radical on the walls of the closed-source chamber, the dot over M_i indicates a time derivative, t_{ij} is the time constant describing the surface reactions of radical i with radical j, U_{sc} is the spacecraft velocity, A_x is the area of the aperture of the closed-source chamber, A_w is the surface area of the closed source chamber, and M_i° is the surface density for a monolayer of species i. The quantity $N_i^a(t)$ is the ambient atmospheric density of the i^{th} radical. The time dependence is explicit to emphasize that the system is driven by the passage of the spacecraft through different altitudes on Titan with varying atmospheric densities. The reaction of species i and j produces a surface density M_{ij} of the product species (for example, $C_6H_5 + H \rightarrow C_6H_6$). We also assume that the gas phase distribution of the product species in the chamber is in steady state with the walls; thus the rate at which gas is desorbed from the walls is equal to the outflow rate from the closed-source aperture:

$$N_{ij}^c \frac{U_w A_x}{4} = \frac{1}{t_{ij}} \frac{M_i}{M_i^\circ} \frac{M_j}{M_j^\circ} \quad (2)$$

where U_w is the thermal velocity at the wall temperature and N_{ij}^c is the gas density in the chamber, i.e., the density measured by the INMS detection system.

[19] Solution of this set of equations gives us a model for the correlation of N_{ij}^c with $N_i^a(t)$. The H and CH_3 densities used in the wall chemistry model come from our photochemical model, described in the next section. The C_6H_5 and C_6H_6 densities are adjusted to fit the data, but the H and CH_3 are held fixed at the values predicted by photochemistry. Our knowledge of surface chemistry for the radicals considered here is too uncertain to permit determination of the chemical time constants from first principles, so we treat them as empirical parameters determined through fits of the model to the T16 data. The results of such a calculation for production of C_6H_6 are shown in Figure 6. A chemical time constant of 15 s for $H + C_6H_5$ provides the best fit to the data.

[20] Adequate fits to the data also require a direct gaseous source of C_6H_6, shown as the dashed line in Figure 6. The required density from this source is 2.5×10^4 cm^{-3}, corresponding to a mole fraction of 1.3×10^{-6} at an altitude of 950 km. Recently *Vuitton et al.* [2007] analyzed the INMS ion data for T5 and determined a mixing ratio of a few ppm for C_6H_6 on Titan's night side, in excellent agreement with the value of 1.3×10^{-6} found

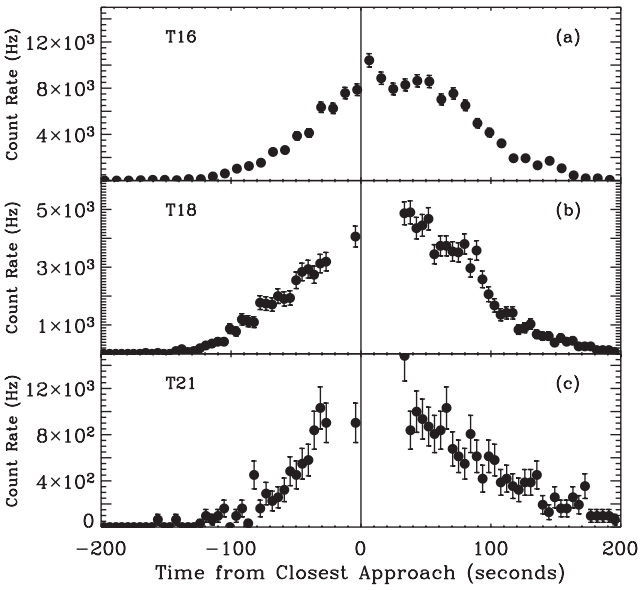

Figure 5. Time dependence of the signal from −200 to 200 s around closest approach for m/z = 78. (a) T16. (b) T18. (c) T21.

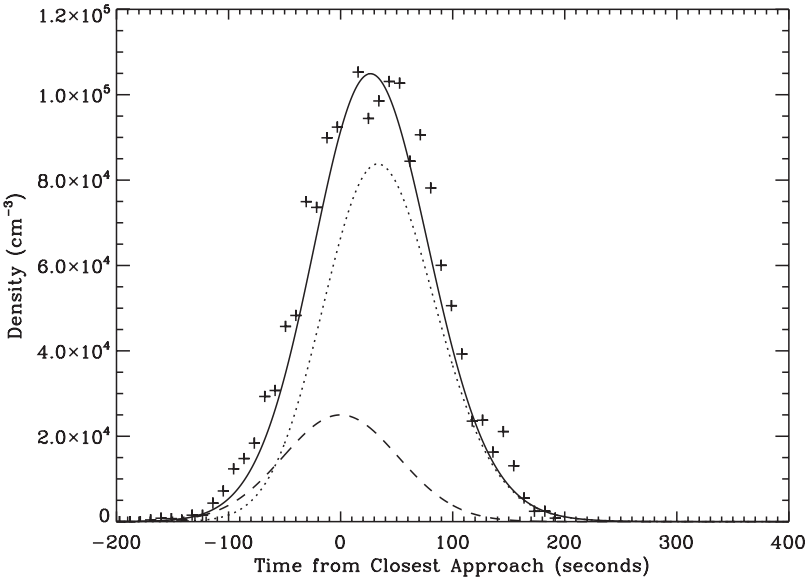

Figure 6. Time dependence model fit for benzene (m/z = 78). Data points represent the density in the closed source obtained during T16 from −200 to 400 s around closest approach. The dotted line corresponds to the recombination of radicals on the walls of the closed source. The dashed line represents the direct gaseous source. The solid line is the sum of the dotted and dashed lines and represents the best fit of the databased on the surface chemistry model.

here. Also, we estimate that the density of benzene in Titan's atmosphere is roughly one third that of phenyl, consistent with the photochemical calculations presented in the next section.

[21] The approach described here cannot be used for passes other than T16 because the spacecraft did not penetrate deep enough into Titan's atmosphere and the signal-to-noise ratio (SNR) of the benzene signal is too low. As a consequence, we cannot explicitly retrieve the benzene density for passes other than T16. Additionally, the signal-to-noise ratio (SNR) of the toluene signal is too low for us to meaningfully constrain the chemical time constant for $C_6H_5 + CH_3$. We therefore adopt the time constant that we determined for $H + C_6H_5$. The fit is adequate but the low SNR of the measurements prevents any further conclusions for this species.

4. Chemical Models

[22] The benzene mole fractions derived in the previous section are many orders of magnitude larger than that derived for the stratosphere. *Coustenis et al.* [2007] report a value varying with latitude from 1.0×10^{-10} to 3.5×10^{-9} at approximately 110 km. This increase of mole fraction with altitude indicates that benzene is formed in the upper atmosphere. The flux, Φ, of a minor constituent is related to the mole fraction, X, through

$$\Phi = -(K + D)N_a \frac{dX}{dr} - DN_aX\left(\frac{1}{H_i} - \frac{1}{H_a}\right) \qquad (3)$$

where, D is the molecular diffusion coefficient, K is the eddy diffusion coefficient, N_a is the atmospheric number density, H_a is the pressure scale height of the background atmosphere and H_i is the diffusive equilibrium scale height of the minor species. Though we have insufficient data to accurately compute dX/dr, the separate measurements in the thermosphere and stratosphere indicate that $dX/dr > 0$ and therefore $\Phi < 0$ and benzene is flowing downward from above. The fact that the abundance of benzene in the thermosphere is larger than in the stratosphere indicates that benzene is synthesized in the thermosphere.

[23] *Lavvas et al.* [2008a, 2008b] developed a one-dimensional radiative-convective/photochemical/microphysical model in order to interpret the composition measurements recently obtained by Cassini. As in previous studies, they find the primary benzene production channel to be the three-body reaction:

$$C_3H_3 + C_3H_3 + M \rightarrow C_6H_6 + M \qquad (k_{10}).$$

[24] The model can almost reproduce the benzene stratospheric mole fraction but it fails to predict the large mole fractions in the thermosphere. The predictions are more than two orders of magnitude less than the observed abundance in the thermosphere reported here. In fact, three-body reactions are extremely inefficient at the low densities in Titan's thermosphere and it seems clear that a chemical scheme that utilizes two-body reactions is required to explain the thermospheric abundance. This raises the question of how benzene is produced in the thermosphere.

[25] We can gain some insight into benzene production by examining the required time constants. The benzene density distribution should only reflect the scale height for a mass of 78 amu if benzene is close to diffusive equilibrium. The time constant characterizing diffusion can be estimated through $t_D = H^2/D$, where H is the benzene scale height and D is the molecular diffusion coefficient. At 1000 km the benzene diffusion coefficient is $D = 3.1 \times 10^9$ cm^2 s^{-1} and the measured scale height is $H = 21$ km, implying a

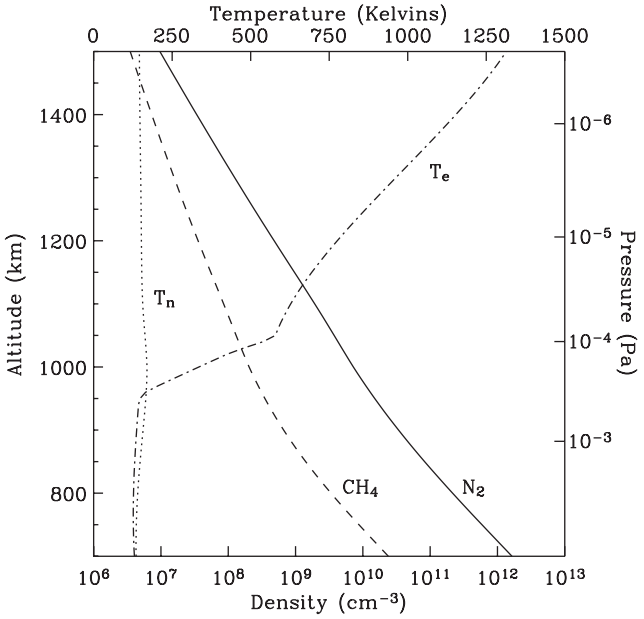

Figure 7. N_2 (solid line) and CH_4 (dashed) density, and neutral T_n (dotted line) and electron temperature T_e (dot-dashed line) used in the ion chemistry model.

diffusion time constant of $t_D = H^2/D \sim 1400$ s. If we assume that the benzene ring is built up by sequential reaction with CH_4 and the intermediary molecules have roughly the same abundance as benzene, then 5 reactions are needed and the required reaction rate is roughly $k \sim 5/N(CH_4)t_D \sim 5 \times 10^{-10}$ cm^3 s^{-1}. If we assume that benzene is synthesized in three reactions involving molecules that contain 2 and 3 carbon atoms present at the ppm level in the atmosphere then the required reaction rate is $k \sim 2 \times 10^{-9}$ cm^3 s^{-1}. These reaction rates are consistent with ion-neutral reaction rates but not neutral-neutral reaction rates, which are much slower. This indicates that the benzene in the ionosphere is likely synthesized by ion chemistry. The likely precursor is protonated benzene, i.e., $C_6H_7^+$, a significant ion in Titan's ionosphere [*Vuitton et al.*, 2007]. Chemical models are discussed in the next subsection, where we argue that protonated and neutral benzene are closely related.

4.1. Ion Chemistry

4.1.1. Description

[26] We use an ion chemistry model based on the 0D model presented by *Vuitton et al.* [2006a, 2007]. The model is extended to 1D in order to allow retrieval of integrated vertical production rates. We use daytime conditions because the solar EUV energy flux is about 10 times the energy flux deposited by magnetospheric electrons [*Cravens et al.*, 2005; *Galand et al.*, 2006] and as a consequence complex species are more efficiently produced on the dayside. The model represents daytime conditions with a local solar zenith angle of 45°, as appropriate for T17. We concentrate on this pass because it is the only one that occurred in sunlight. Unfortunately, the neutral data for T17 were compromised and we cannot directly compare benzene and $C_6H_7^+$ densities.

[27] The background atmosphere is derived from an empirical model based on the INMS data for the thermosphere [*Müller-Wodarg et al.*, 2008], CIRS results for the stratosphere [*Vinatier et al.*, 2007], and Huygens results for the troposphere [*Fulchignoni et al.*, 2005; *Niemann et al.*, 2005], as described in the work of *Yelle et al.* [2008]. Profiles of N_2 and CH_4 densities and the atmospheric temperature profile are presented on Figure 7. The densities and temperature are representative of the spacecraft location at C/A for T17. To calculate the relative production rates of N_x^+ (x = 1,2) and CH_y^+ (y = 0–4), we use the photoionization cross sections of *Samson et al.* [1987] and *Stolte et al.* [1998] for N_2, and of *Lee and Chiang* [1983] and *Samson et al.* [1989] for CH_4. The solar flux is based on the solar EUV flux model for Aeronomic Calculations (EUVAC), scaled to the location of Titan [*Richards et al.*, 1994a, 1994b]. We can be fairly confident that ionization by energetic magnetospheric electrons and ions is small compared with solar ionization [*Cravens et al.*, 2005; *Galand et al.*, 2006] and is therefore neglected. We assume chemical equilibrium for the ion species. This is a good assumption on the dayside and at the altitudes that primarily concern us here.

[28] The chemical network includes ~150 ions containing up to 9 heavy atoms (carbon and nitrogen), ~40 neutrals and ~1250 ion-molecule reactions. The densities of heavier neutrals are fixed in the model at values either measured by INMS in the neutral mode or determined from the observed ion densities [*Vuitton et al.*, 2007]. Reaction rate constants and products are mostly retrieved from existing compilations of experimental data [*Anicich*, 1993; *Anicich and McEwan*, 1997; *McEwan and Anicich*, 2007]. Titan's ionospheric chemistry is driven by proton exchange reactions where ionization flows from neutrals having small proton affinities (PA) to neutrals having larger PA [*Fox and Yelle*, 1997; *Vuitton et al.*, 2006a]. We assume that CH_5^+, $C_2H_5^+$ and $HCNH^+$ readily exchange a proton with neutrals having a higher proton affinity. When the reaction has not been studied, we assume the rate constant to be equal to the collision rate and calculate Langevin rates at 300 K. Use of Langevin rates for a temperature of 150 K lead only to minor changes in the modeled ion densities. Ion-electron recombination rates are retrieved from the literature. When the electron temperature dependence has not been determined, we assume the rate constant to be proportional to $T_e^{-0.7}$ and when no data are available, we estimate the recombination rate to be equal to $7 \times 10^{-7} \times (300/T_e)^{0.7}$ cm^3 s^{-1}. Thermal electron temperature, as measured by the Cassini Radio Plasma Wave Spectrometer (RPWS) during the T17 encounter, are shown on Figure 7 [J.-E. Wahlund, personal communication, 2007].

[29] According to our chemical model C_6H_6 is produced primarily from the sequence of reactions presented on Figure 8 and listed in Table 2. For most reactions, the structure of the ions produced is not known because experimental data are usually based on mass spectrometry. The form of $C_6H_5^+$ and $C_6H_7^+$, whether cyclic or not, likely determines if electron recombination produces benzene or another C_6H_6 isomer. The reaction $C_4H_3^+ + C_2H_2 \rightarrow C_6H_5^+ + h\nu$ (k'_{11}) produces 2 isomers, one cyclic and one linear. The ground state isomer c-$C_6H_5^+$ is reactive but l-$C_6H_5^+$ is not [*Scott et al.*, 1997]. Generally, when there is radiative stabilization, ring closure occurs and the cyclic form dominates [*McEwan et al.*, 1999]. Accordingly, we assume that $C_6H_5^+$ and $C_6H_7^+$ are cyclic and we use rate constants corresponding to c-$C_6H_5^+$ and c-$C_6H_7^+$, if available.

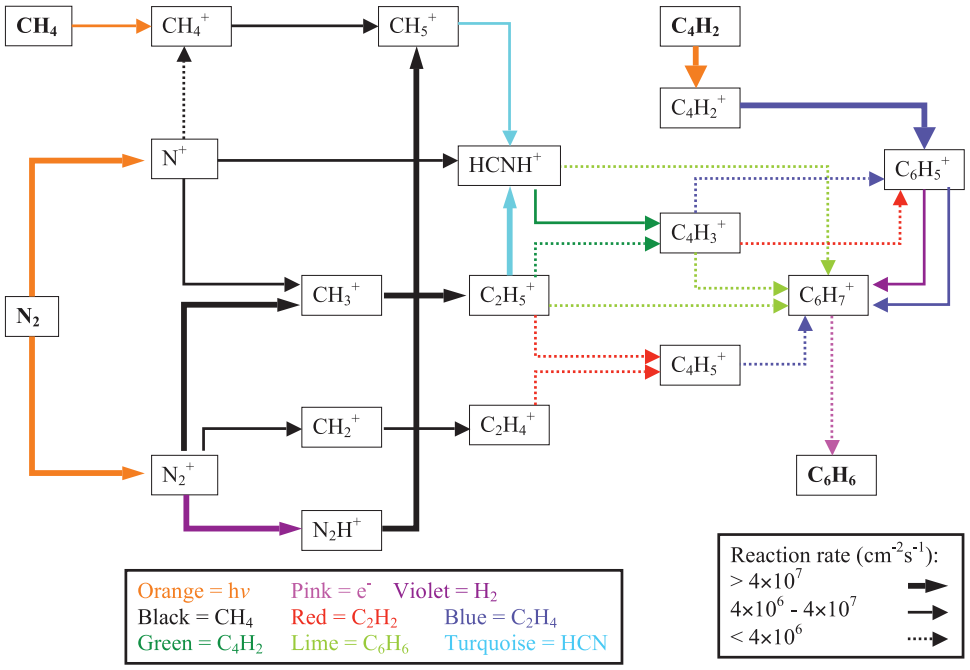

Figure 8. Flowchart of the principal ion chemistry reactions for benzene formation.

[30] The electron recombination rate of c-$C_6H_7^+$ has been measured for electron temperatures of 300 to 800 K but products are not known [*McLain et al.*, 2004]. We assume that benzene and H are the only products. This is a key assumption in our model and laboratory measurements are desperately needed. It is also possible that products other than benzene would be quickly converted by subsequent reactions to benzene. Other recombination of heavy ions may also lead to benzene production, or to molecules that get converted to benzene, but these possibilities are not considered here.

4.1.2. Results

[31] The calculated altitude profiles for some key ions in benzene production are compared to the measured densities from T17 inbound in Figures 9a–9b. For the lighter species (Figure 9a), the model results are in good agreement with the observations, suggesting that solar UV deposition and primary ion chemistry are well described by the model. For

Table 2. Principal Ion Reactions for Benzene Formation

R#	Reaction	Rate Constant[a]	Reference
k'_1	$CH_2^+ + CH_4 \rightarrow C_2H_4^+ + H_2$	9.1×10^{-10}	[*Anicich*, 1993]
k'_2	$CH_3^+ + CH_4 \rightarrow C_2H_5^+ + H_2$	1.1×10^{-9}	[*Anicich et al.*, 2003]
k'_3	$CH_4^+ + CH_4 \rightarrow CH_5^+ + CH_3$	1.1×10^{-9}	[*Anicich*, 1993]
k'_4	$CH_5^+ + HCN \rightarrow HCNH^+ + CH_4$	4.1×10^{-9}	estimate
k'_5	$C_2H_4^+ + C_2H_2 \rightarrow C_4H_5^+ + H$	1.9×10^{-10}	[*Anicich*, 1993]
k'_6	$C_2H_5^+ + C_2H_2 \rightarrow C_4H_5^+ + H_2$	1.2×10^{-10}	[*Kim et al.*, 1977]
k'_7	$C_2H_5^+ + C_4H_2 \rightarrow C_4H_3^+ + C_2H_4$	1.0×10^{-9}	estimate
k'_8	$C_2H_5^+ + C_6H_6 \rightarrow C_6H_7^+ + C_2H_4$	1.1×10^{-9}	estimate
k'_9	$C_2H_5^+ + HCN \rightarrow HCNH^+ + C_2H_4$	2.7×10^{-9}	[*Mackay et al.*, 1980]
k'_{10}	$C_4H_2^+ + C_2H_4 \rightarrow C_6H_5^+ + H$	7.2×10^{-10}	[*Anicich et al.*, 2006]
k'_{11}	$C_4H_3^+ + C_2H_2 \rightarrow C_6H_5^+ + hv$	2.2×10^{-10}	[*Anicich*, 1993]
k'_{12}	$C_4H_3^+ + C_2H_4 \rightarrow C_6H_5^+ + H_2$	1.2×10^{-10}	[*Anicich et al.*, 2006]
k'_{13}	$C_4H_3^+ + C_6H_6 \rightarrow C_6H_7^+ + C_4H_2$	1.3×10^{-9}	[*Deakyne et al.*, 1987; *Lifshitz and Weiss*, 1980]
k'_{14}	$C_4H_5^+ + C_2H_4 \rightarrow C_6H_7^+ + H_2$	7.3×10^{-11}	[*Anicich et al.*, 2006]
k'_{15}	$C_6H_5^+ + H_2 \rightarrow C_6H_7^+ + hv$	6.0×10^{-11}	[*McEwan et al.*, 1999]
k'_{16}	$C_6H_5^+ + C_2H_4 \rightarrow C_6H_7^+ + C_2H_2$	1.0×10^{-10}	[*Anicich et al.*, 2006]
k'_{17a}	$N^+ + CH_4 \rightarrow CH_3^+ + NH$	5.8×10^{-10}	[*Anicich*, 1993]
k'_{17b}	$N^+ + CH_4 \rightarrow CH_4^+ + N$	5.8×10^{-11}	[*Anicich*, 1993]
k'_{17c}	$N^+ + CH_4 \rightarrow HCNH^+ + H_2$	4.1×10^{-10}	[*Anicich*, 1993]
k'_{18}	$N_2^+ + H_2 \rightarrow N_2H^+ + H$	2.0×10^{-9}	[*Anicich*, 1993]
k'_{19a}	$N_2^+ + CH_4 \rightarrow CH_2^+ + N_2 + H_2$	1.0×10^{-10}	[*Anicich et al.*, 2006]
k'_{19b}	$N_2^+ + CH_4 \rightarrow CH_3^+ + N_2 + H$	1.0×10^{-9}	[*Anicich et al.*, 2006]
k'_{20}	$N_2H^+ + CH_4 \rightarrow CH_5^+ + N_2$	8.9×10^{-10}	[*Burt et al.*, 1970]
k'_{21}	$HCNH^+ + C_4H_2 \rightarrow C_4H_3^+ + HCN$	1.8×10^{-9}	[*Petrie et al.*, 1991]
k'_{22}	$HCNH^+ + C_6H_6 \rightarrow C_6H_7^+ + HCN$	1.1×10^{-9}	estimate
α_1	$C_6H_7^+ + e^- \rightarrow C_6H_6 + H$	$2.4 \times 10^{-6}\ (300/T_e)^{1.3}$	[*McLain et al.*, 2004]

[a]Bimolecular rate constant ($cm^3\ s^{-1}$).

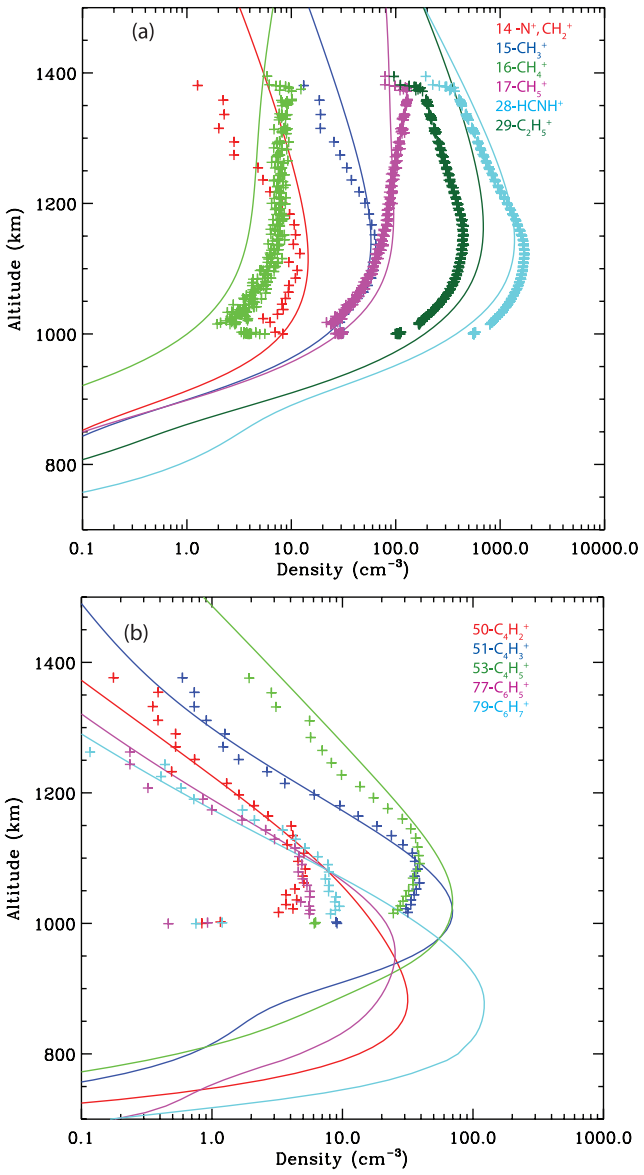

Figure 9. Observed vertical profiles of some key ions during T17 inbound. The solid lines represent the predictions of the ion chemistry model. (a) m/z = 14, 15, 16, 17, 28, 29. (b) m/z = 50, 51, 53, 77, 79. The $C_4H_2^+$ curve has been scaled by a factor of 10.

the heavier species (Figure 9b), the model reproduces the data down to ~1100 km but at lower altitude, the model predictions systematically overestimates the observed ion densities. The modeled ion density peak decreases in altitude with the ion mass because of the smaller scale height of the heavier neutrals. However, the observed ion density peak is located around 1100 km for all the species, independently of their mass. Observational effects might cause this unexpected behavior. Because the width of the velocity distribution of heavy ions is narrower than the width of the velocity distribution of lighter ions, any mistuning of the lenses of the mass spectrometer caused by strong winds, etc. would be reflected as an underestimation of the higher masses density.

[32] Some chemistry is possibly missing in our model but it is not clear if this could explain the discrepancy observed at low altitude. The Electron Spectrometer (ELS), one of Cassini Plasma Spectrometer (CAPS) instruments, detected negative ions below ~1150 km in all Titan flybys [*Coates et al.*, 2007]. Even if the negative ion density were a substantial fraction of the electron density, positive-negative ion recombination would not substantially reduce the positive ion density, because recombination with negative ions is about 10 times slower than recombination with electrons. Also, if the chemistry is complex enough to lead to the formation of nanometer size aerosols, as suggested by the detection of high molecular mass (>10,000 amu) negative ions during T16 [*Coates et al.*, 2007; *Waite et al.*, 2007], ion reactions on the surface of aerosols could act as a sink for ions. Generally, addition reactions of heavier ions are faster than addition reactions of lighter ions because of their higher number of vibrational modes required to redistribute the energy liberated by the reaction. Better observational constrain on both negative ions and heavier molecular mass positive ions are required before these species can be taken into account in the model.

[33] Our model cannot reproduce the observed ion density at m/z = 50. As explained in the work of *Vuitton et al.* [2007], this mass is attributed to $C_4H_2^+$ but ion-molecule reactions do not efficiently produce $C_4H_2^+$. Here we improve the previous model by including direct photoionization of C_4H_2. We use the C_4H_2 mole fraction inferred from the $C_4H_3^+$ density, the photoionization cross sections of *Cool et al.* [2005] and the solar flux described previously. This process forms a significant amount of $C_4H_2^+$ but the modeled density profile still falls short by about one order of magnitude. As represented on Figure 8 and discussed in the next paragraph, $C_4H_2^+$ is an important intermediate in $C_6H_7^+$ formation and in order to estimate the benzene production rate it is crucial that the model accurately predicts the $C_4H_2^+$ density. Fragmentation of heavier ions could possibly produce $C_4H_2^+$ ions but without further experimental constraints, it is not possible to include such reactions in the model. As a consequence, we scale the $C_4H_2^+$ production rate by a factor of 10 in order to get a forced agreement between observed and calculated $C_4H_2^+$ densities, as showed on Figure 9b.

[34] On the night-side, *Vuitton et al.* [2007] showed that because the ionization rate by magnetospheric electrons is small, $C_6H_7^+$ is mostly produced by proton exchange reactions between the major ions and C_6H_6, and lost by electron recombination to form back C_6H_6. As a consequence, $C_6H_7^+$ is constantly recycled and ion chemistry does not contribute to a net production of C_6H_6. However, on the dayside, N_2 and CH_4 are rapidly photoionized and $C_6H_7^+$ is efficiently produced by ion chemistry reactions. Figure 9b shows the altitude profile for $C_6H_7^+$ ions on T17 inbound. The lower peak in the $C_6H_7^+$ density is from

$$C_6H_5^+ + C_2H_4 \rightarrow C_6H_7^+ + C_2H_2 \qquad (k'_{16}),$$

and

$$C_6H_5^+ + H_2 \rightarrow C_6H_7^+ + h\nu \qquad (k'_{15}),$$

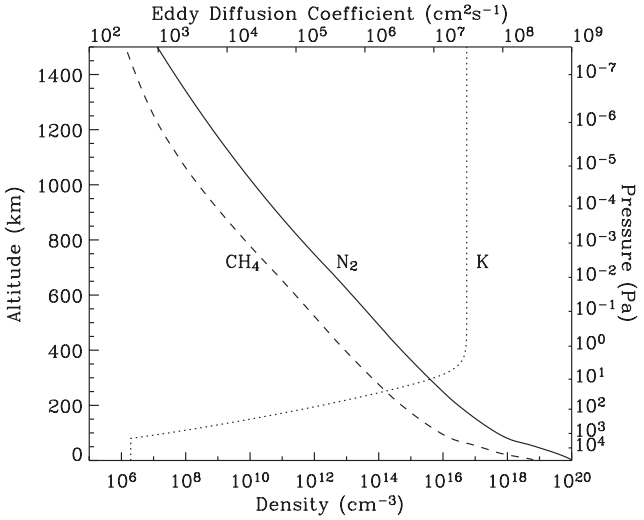

Figure 10. N_2 (solid line), CH_4 (dashed line) and eddy diffusion K (dotted line) profiles used in the neutral chemistry model.

with a total column production rate of 3.2×10^7 cm^{-2} s^{-1}. $C_6H_5^+$ comes primarily from

$$C_4H_2^+ + C_2H_4 \rightarrow C_6H_5^+ + H \qquad (k'_{10}),$$

so it is necessary to accurately match the $C_4H_2^+$ density, as discussed above. The upper peak in the $C_6H_7^+$ density is from

$$C_4H_5^+ + C_2H_4 \rightarrow C_6H_7^+ + H_2 \qquad (k'_{14}).$$

with a total column production rate of 1.6×10^6 cm^{-2} s^{-1}. Benzene is subsequently produced by electron recombination of $C_6H_7^+$:

$$C_6H_7^+ + e^- \rightarrow C_6H_6 + H \qquad (\alpha_1).$$

[35] The measured electron density and temperature, the density of $C_6H_7^+$, and the recombination coefficient imply a C_6H_6 production rate of 1.0×10^{-1} cm^{-3} s^{-1} at 1000 km. The column-integrated production rate at a solar zenith angle of 45° derived from the ionospheric model is 3.7×10^7 cm^{-2} s^{-1}, which corresponds to a globally averaged rate of 1.3×10^7 cm^{-2} s^{-1}. These rates and all the subsequent column integrated rates are referred to the surface. Approximately 95% of the benzene production occurs below the altitude for which we have measurements and thus represents an extrapolation based on our calculation of solar ionization and our chemical reaction list. Nevertheless, our calculated ionospheric production rate is sufficient to produce large benzene densities in Titan's upper atmosphere, of the same order as those measured by the INMS.

4.2. Neutral Chemistry

4.2.1. Description

[36] To investigate this further we have constructed a neutral photochemical/diffusion model for the distribution of benzene. The model includes eddy and molecular diffusion, photolysis, and chemistry. Our photolysis rates are based on a solar spectrum obtained with the EUV flux model for Aeronomic Calculations (EUVAC), scaled to the location of Titan [*Richards et al.*, 1994a, 1994b]. We adopt a solar zenith angle of 60° and divide the rates by a factor of 2, to represent a global average. The temperature and total density are representative of the equatorial region, as determined in the empirical model of *Müller-Wodarg et al.* [2008]. The N_2 and CH_4 densities are presented on Figure 10 and the temperature profile is shown in the work of *Yelle et al.* [2008]. Molecular diffusion coefficients are taken from measurements presented in the literature if possible [*Mason and Marrero*, 1970] or calculated from molecular force constants using the standard approach [*Hirschfelder et al.*, 1964] if no measurements are available. We found no measurements for the diffusion coefficient of benzene in N_2. We calculate that the diffusion coefficient has a value of $DN = 2.3 \times 10^{19}$ cm^{-1} s^{-1} at a temperature of 150 K. The eddy mixing profile is constrained by INMS measurements of the ^{40}Ar distribution in the upper atmosphere and by CIRS measurements of the C_2H_6 distribution in the stratosphere [*Yelle et al.*, 2008] and is presented on Figure 10. The 1D chemical-diffusion model does not include ions or ion chemistry. We specify an ion-molecule production rate for benzene consistent with that inferred from our ion-molecule reaction model. The production rate is specified as a Chapman production profile with a peak at 830 km of 1.3 cm^{-3} s^{-1} and a scale height of 75 km. The column-integrated production rate is 7×10^6 cm^{-2} s^{-1}, which is on the same order as the rate of 1.3×10^7 cm^{-2} s^{-1} predicted by the ion chemistry model.

[37] The neutral chemical network is based on the reaction list presented in the work of *Vuitton et al.* [2006b]. It consists of 40 hydrocarbon species, ~130 neutral-neutral reactions and ~40 photoreactions. Chemical reactions and photolysis of C_6H_6 (benzene), C_7H_8 (toluene), C_8H_{10} (ethylbenzene) and their associated radicals is described explicitly. Oxygen and nitrogen bearing species are not abundant enough to significantly affect the hydrocarbon densities and in order to avoid a significant increase of the chemical network complexity, we do not consider the nitrogen or oxygen chemistry in this study. Molecules with more than 6 carbon atoms are assumed to ultimately form soot and are no longer involved in the chemistry. Because we expect benzene rings to be conserved, complex species produced by reaction of C_6H_5 or other aromatic radicals are included in a sub-category of soot called "rings". "aromatics" refers to C_6H_6, C_7H_8, C_8H_{10} and "rings", "solid aromatics" refers to condensed C_6H_6, C_7H_8, C_8H_{10}, and "rings". Reactions relevant to benzene production and destruction are listed in Table 3.

[38] Besides the ionospheric source, we include production through neutral chemistry and extend the chemical network considered in previous models. There have been three recent studies of the kinetics of the propargyl (C_3H_3) self-reaction at 295 K, reporting rate coefficients of $\sim 4 \times 10^{-11}$ cm^3 s^{-1} [*Atkinson and Hudgens*, 1999; *De Sain and Taatjes*, 2003; *Fahr and Nayak*, 2000]. These new results seem to supersede the threefold higher value obtained by *Morter et al.* [1994]. This rate coefficient is independent of total pressure and buffer choice (Ar, He, N_2) over the pressure range 3–133 mbar, indicating that the

Table 3. Principal Neutral Reactions for Benzene Formation

R#	Reaction	Rate Constant[a]	T Range[b]	Reference
k_1	$H + C_6H_5 \rightarrow C_6H_6$	$\mathbf{1.7 \times 10^{-23}\ T^{-1.8}}$	$300^{-10}00$	10 k_0(H + CH_3) [*Baulch et al.*, 1994]
		$6.9 \times 10^{-11}\ T^{+0.15}$	200–2000	[*Harding et al.*, 2005]
k_2	$CH_3 + C_6H_5 \rightarrow C_7H_8$	$\mathbf{2.2 \times 10^{-15}\ T^{-3.75}\ exp(-494/T)}$	200–1350	10 k_0(CH_3 + CH_3) [*Wang et al.*, 2003]
		2.3×10^{-11} exp(−23/T)	$300^{-9}80$	[*Tokmakov et al.*, 1999]
k_3	$C_2 + C_6H_6 \rightarrow C_8H_5 + H$	5.2×10^{-10}	300	[*Reisler et al.*, 1980]
k_4	$C_2H + C_4H_6 \rightarrow C_6H_6 + H$	3.0×10^{-10}	104–296	[*Nizamov and Leone*, 2004]
k_5	$C_2H + C_6H_6 \rightarrow C_8H_6 + H$	$9.1 \times 10^{-10}\ T^{-0.18}$	105–298	[*Goulay and Leone*, 2006]
k_{6a}	$C_2H_3 + C_4H_3 \rightarrow C_6H_6$	$\mathbf{2.2 \times 10^{-15}\ T^{-3.75}\ exp(-494/T)}$	200–1350	10 k_0(CH_3 + CH_3) [*Wang et al.*, 2003]
		4.8×10^{-10} exp(−411/T)	700–1300	[*Duran*, 1988]
k_{6b}	$C_2H_3 + C_4H_3 \rightarrow C_2H_4 + C_4H_2$	1.2×10^{-11}	298	k(C_2H_3 + C_2H_3) [*Fahr et al.*, 1991]
k_{6c}	$C_2H_3 + C_4H_3 \rightarrow C_2H_2 + C_4H_4$	1.2×10^{-11}	298	k(C_2H_3 + C_2H_3) [*Fahr et al.*, 1991]
k_{7a}	$C_2H_3 + C_4H_5 \rightarrow C_6H_8$	$\mathbf{2.2 \times 10^{-15}\ T^{-3.75}\ exp(-494/T)}$	200–1350	10 k_0(CH_3 + CH_3) [*Wang et al.*, 2003]
		1.2×10^{-10}	298	k_∞ (C_2H_3 + C_2H_3) [*Fahr et al.*, 1991]
k_{7b}	$C_2H_3 + C_4H_5 \rightarrow C_2H_4 + C_4H_4$	1.2×10^{-11}	298	k(C_2H_3 + C_2H_3) [*Fahr et al.*, 1991]
k_{7c}	$C_2H_3 + C_4H_5 \rightarrow C_2H_2 + C_4H_6$	1.2×10^{-11}	298	k(C_2H_3 + C_2H_3) [*Fahr et al.*, 1991]
k_{8a}	$C_2H_3 + C_6H_5 \rightarrow C_8H_8$	$\mathbf{2.2 \times 10^{-15}\ T^{-3.75}\ exp(-494/T)}$	200–1350	10 k_0(CH_3 + CH_3) [*Wang et al.*, 2003]
		1.2×10^{-10}	298	k_∞ (C_2H_3 + C_2H_3) [*Fahr et al.*, 1991]
k_{8b}	$C_2H_3 + C_6H_5 \rightarrow C_2H_4 + C_6H_4$	1.2×10^{-11}	298	k(C_2H_3 + C_2H_3) [*Fahr et al.*, 1991]
k_{8c}	$C_2H_3 + C_6H_5 \rightarrow C_2H_2 + C_6H_6$	1.2×10^{-11}	298	k(C_2H_3 + C_2H_3) [*Fahr et al.*, 1991]
k_{9a}	$C_2H_5 + C_6H_5 \rightarrow C_8H_{10}$	$2.2 \times 10^{-15}\ T^{-3.75}$ exp(−494/T)	200–1350	10 k_0(CH_3 + CH_3) [*Wang et al.*, 2003]
		1.2×10^{-10}	298	k_∞ (C_2H_3 + C_2H_3) [*Fahr et al.*, 1991]
k_{9b}	$C_2H_5 + C_6H_5 \rightarrow C_2H_6 + C_6H_4$	1.2×10^{-11}	298	k(C_2H_3 + C_2H_3) [*Fahr et al.*, 1991]
k_{9c}	$C_2H_5 + C_6H_5 \rightarrow C_2H_4 + C_6H_6$	1.2×10^{-11}	298	k(C_2H_3 + C_2H_3) [*Fahr et al.*, 1991]
k_{10}	$C_3H_3 + C_3H_3 \rightarrow C_6H_6$	$\mathbf{2.2 \times 10^{-15}\ T^{-3.75}\ exp(-494/T)}$	200–1350	10 k_0(CH_3 + CH_3) [*Wang et al.*, 2003]
		4.0×10^{-11}	295	[*Fahr and Nayak*, 2000]
k_{11}	$C_6H_5 + C_6H_5 \rightarrow C_{12}H_{10}$	$\mathbf{2.2 \times 10^{-15}\ T^{-3.75}\ exp(-494/T)}$	200–1350	10 k_0(CH_3 + CH_3) [*Wang et al.*, 2003]
		2.3×10^{-11} exp(−56/T)	295	[*Park and Lin*, 1997]

[a]Plain: bimolecular rate constant ($cm^3\ s^{-1}$) /Bold: trimolecular rate constant ($cm^6\ s^{-2}$).
[b]Temperature range for which the reaction has been studied (K).

reaction is at the high-pressure limit in the experimental conditions. The rate coefficient exhibits a slight temperature dependence from 373 to 1000 K [*Giri et al.*, 2003; *Shafir et al.*, 2003] but no measurement is available below room temperature. As a consequence, we used a temperature independent rate coefficient in our model. The reaction rate has never been measured in the low-pressure range. We assume that it is equal to 10 times the recombination rate of methyl (CH_3) radicals because of the higher number of channels available to redistribute the excess energy. We base our estimate on the CH_3 recombination rate of *Wang et al.* [2003], which was obtained from a combination of theoretical and experimental investigations down to 200 K.

[39] The C_6H_6 produced in the reaction of propargyl radicals is not necessarily in the form of benzene. *Fahr and Nayak* [2000] analyzed products for propargyl recombination at T = 298 K and P = 67 mbar. They detected two linear C_6H_6 (1,5−hexadiyne and 1,2−hexadiene−5yne) with yields of 60 and 25%, respectively and a third unidentified isomer. *Howe and Fahr* [2003] performed product studies at a pressure range of 27 mbar to 933 mbar and at a temperature range of 295−623 K. The same two linear and three new cyclic C_6H_6 isomers (dimethylenecyclobutene, fulvene and benzene) were identified. Benzene was a major product particularly at low pressure (∼25%). The authors suggest that extrapolation of the product yield to low pressures (<15 mbar) gives a yield of about 40%, irrespective of the temperature. This is in qualitative agreement with the theoretical results of *Miller and Klippenstein* [2003]. In the absence of any data concerning the isomerization or reactivity of the different C_6H_6 isomers, we assume that cyclization quickly occurs and that the only C_6H_6 product is benzene.

[40] Reactions of the C_3H_2, C_3H_3, C_4H_3, C_4H_5 and C_6H_5 radicals with C_2H_2 have been considered as a potential source of C_6H_6 [*Lebonnois*, 2005; *Wilson et al.*, 2003]. However, a large energy barrier makes them unimportant at low temperatures [*Moses et al.*, 2005; *Vuitton et al.*, 2006b] and we do not consider these reactions in our model. Instead, we include in the chemical network the reaction between C_2H and 1,3-butadiene (C_4H_6). The reaction is fast ($k = 3 \times 10^{-10}\ cm^3\ s^{-1}$) and 1,3-butadiene is efficiently produced in the recombination of C_2H_3 radicals [*Fahr et al.*, 1991; *Nizamov and Leone*, 2004]. The products have not been determined but it is usually believed that the reaction of C_2H with unsaturated molecules proceeds via attack of a π-orbital followed by rapid loss of an H atom by the energized complex initially formed. It follows that the product of reaction k_4 is most probably C_6H_6.

[41] The most important chemical loss process for benzene is photolysis, which extends as far as 270 nm [*Pantos et al.*, 1978]. To estimate the photolysis rate, we use the cross section published by *Koch and Otto* [1972] and *Pantos et al.* [1978]. However, the photolysis of benzene is complicated, and the products are not completely characterized. Deactivation of the excited electronic states formed by absorption of ultraviolet photons lead to a transient highly excited state of the ground electronic state (C_6H_6*). This state has a lifetime of up to 2 ms and subsequently fragments into the photodissociation products [*Tsai et al.*, 2000]. C_6H_6* can also be deactivated by collisions with N_2 [*Nakashima and Yoshihara*, 1982]. As a consequence, C_6H_6* can be collisionally stabilized if the background atmospheric pressure is high enough, whereas dissociation occurs if collisions are rare. Our model

Table 4. Formation and Loss Processes of Hot Benzene C_6H_6*

R#	Reaction	Rate Constant[a]	Lifetime (s) 900 km	Lifetime (s) 300 km	Reference
J_1	$C_6H_6 + h\nu \rightarrow C_6H_6$*	–	2×10^5	5×10^5	[*Koch and Otto*, 1972; *Pantos et al.*, 1978]
k_1*	C_6H_6* $\rightarrow C_6H_5 + H$	**>5.0 × 10²**	$<2 \times 10^{-3}$	$<2 \times 10^{-3}$	[*Tsai et al.*, 2000]
J*	C_6H_6* + h$\nu \rightarrow$ products	–	$\sim 2 \times 10^5$	$\sim 5 \times 10^5$	estimated equal to J_1
k_2*	C_6H_6* + $N_2 \rightarrow C_6H_6$	5.5×10^{-13}	3×10^1	6×10^{-5}	[*Nakashima and Yoshihara*, 1982]
k_3*	C_6H_6* + $C_xH_y \rightarrow$ products	$<5.5 \times 10^{-10}$	$>1 \times 10^0$	$>3 \times 10^{-6}$	estimate[b]

[a]Plain: bimolecular rate constant ($cm^3\ s^{-1}$) /Bold: unimolecular rate constant (s^{-1}).
[b]C_xH_y taken as CH_4 (2% N_2). The lifetime obtained is a lower limit since C_6H_6* may only react with heavier, less abundant species.

explicitly calculates the C_6H_6* density. The lifetime of 2 ms and the de-excitation coefficient (k_2*) imply that dissociation occurs above 350 km and stabilization below. C_6H_6* could also react with other molecules (k_3*) or absorb a photon (J*), leading to different products from single-photon absorption. We assume a reaction rate constant k_3* of 5.5×10^{-10} $cm^3\ s^{-1}$ and a dissociation coefficient J* equal to that of benzene. Estimations of the efficiency of these processes at 900 and 200 km are summarized in Table 4.

[42] The main contribution to the photolysis rate comes from the peak in the absorption cross section near 220 nm, which is also the region used in the laboratory studies of dissociation pathways. In the near ultraviolet, we assume photodissociation products to be exclusively C_6H_5 and H [*Kislov et al.*, 2004]. At shorter wavelength ($\lambda < 135$ nm), ionization represents more than 50% of the total absorption [*Person*, 1965; *Rennie et al.*, 1998] but both ion and neutral products are ill-defined. The fact that the benzene photoabsorption cross section extends to long wavelengths coupled with the rapid increase in solar flux with increasing wavelength implies that 80–90% of the absorption occurs at wavelengths above 180 nm. As a consequence, we make the assumption that photodissociation products are identical over the whole spectral range.

[43] The fate of the C_6H_5 produced by benzene photolysis is to reform benzene through

$$C_6H_5 + H + M \rightarrow C_6H_6 + M \qquad (k_1),$$

or to produce toluene through

$$C_6H_5 + CH_3 + M \rightarrow C_7H_8 + M \qquad (k_2).$$

[44] There is little kinetic data on the reaction of C_6H_5 with other species. Since C_6H_5 is a rather low energy radical (ΔH_f = 339 kJ/mol), we consider it unlikely that it could react with stable species in the atmosphere, and hypothesize that the other main losses are through radical-radical reactions such as

$$C_6H_5 + C_2H_3 + M \rightarrow C_8H_8 + M \qquad (k_{8a}),$$

or

$$C_6H_5 + C_2H_5 + M \rightarrow C_8H_{10} + M \qquad (k_{9a}).$$

[45] We assume that the rate for these reactions is 1.2×10^{-10} $cm^{-3}\ s^{-1}$, based on analogy with

$$C_2H_3 + C_2H_3 + M \rightarrow C_4H_6 + M.$$

4.2.2. Results

[46] In Figure 11a, the vertical profiles of the principal neutrals are displayed for a simulation using the solar flux, chemical network and eddy diffusion coefficient stated previously. The ^{40}Ar profile is compared to the INMS [*Yelle et al.*, 2008] and GCMS [*Niemann et al.*, 2005] results in the upper and lower atmosphere, respectively. The C_2H_2, C_2H_6 and C_4H_2 profiles are compared to the CIRS measurements at 15°S [*Vinatier et al.*, 2007]. The model matches closely both the measured ^{40}Ar and C_2H_6 mole fractions, thus validating the choice of eddy diffusion coefficient. The C_2H_2 profile is in extremely good agreement with the observations as well. The C_4H_2 profile is a factor of 2–3 too high, but that is still a fairly good agreement considering the numerous uncertainties in the C_4H_2 formation and loss processes [*Vuitton et al.*, 2006b].

[47] The vertical profiles of the aromatic species are displayed in Figure 11b. Averages of the INMS C_6H_x mole fractions over the 12 passes presented in Table 1 as well as the C_6H_6 mole fraction retrieved by CIRS at 15°S [*Coustenis et al.*, 2007] are plotted for comparison. Figure 11c shows the vertical profiles of the principal radicals and Figure 12 the rates of the reactions that have a significant impact on the benzene mole fraction. The calculated profiles reproduce the main characteristics of the measurements. Near 900 km, electron recombination of $C_6H_7^+$ forms C_6H_6 (α_1), which is rapidly depleted by photolysis (J_1) to produce C_6H_5. The C_6H_5 density in the model at 1000 km is 2.0×10^4 cm^{-3}, corresponding to a mole fraction of 1.4×10^{-6}, as displayed in Figure 11c. This is 2.5 times the benzene density at the same altitude. The INMS observations reveal a mole fraction of C_6H_x of $\sim 2 \times 10^{-6}$ at 1000 km in good agreement with the model results. Other abundant radicals at ~1000 km include hydrogen (H) and methyl (CH_3) radicals. They are produced mainly through methane photolysis above 700 km.

[48] As shown in Figure 12, photolysis is the main loss for benzene around 900 km. C_6H_5, the main photodissociation product, diffuses downward and is converted to heavier aromatics in the 350–800 km region (k_2, k_{8a}, k_{9a}). This process is responsible for the rapid decrease in benzene mole fraction below 900 km shown in Figure 11b. As the pressure increases, stabilization of the transient benzene becomes more important and it becomes comparable to its dissociation lifetime (k_1*/k_2* ~ 1) at a density of

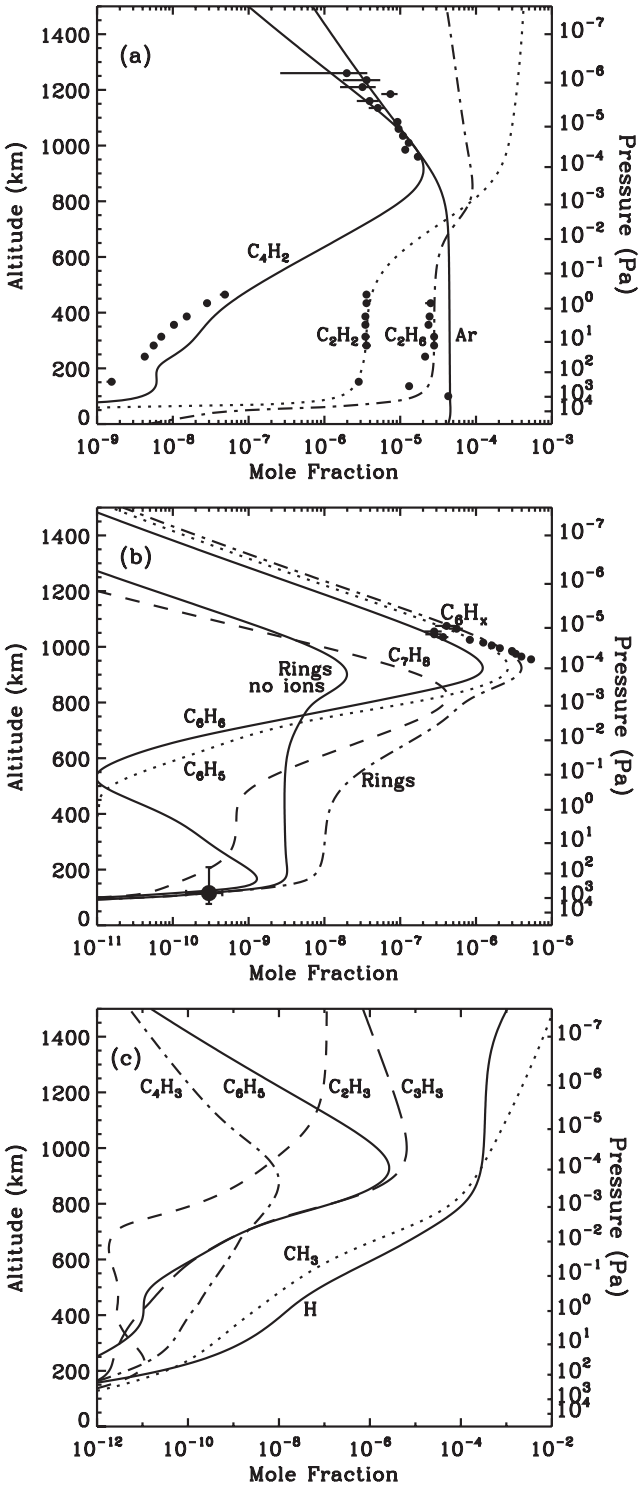

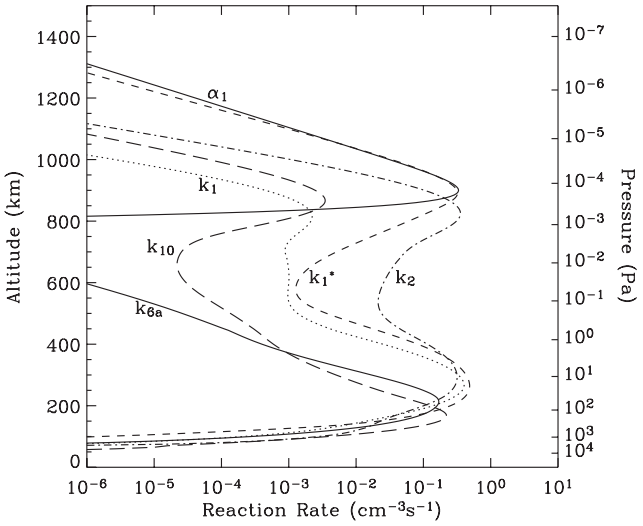

Figure 12. Modeled reaction rates for some key reactions. Labels refer to the reactions listed in Tables 2, 3 and 4.

10^{15} cm^{-3} (~350 km). Thus in the lower atmosphere, stabilization of the transient state is the dominant process. Moreover, at 350 km, the recombination of H and C_6H_5 (k_1) becomes equal to the photolysis rate and destruction of C_6H_6 by photolysis stops. Below 300 km, C_6H_6 is created by recombination of C_2H_3 and C_4H_3 (k_{6a}), and C_3H_3 (k_{10}), producing the low altitude peak in C_6H_6 density observed by CIRS. The mole fraction in the lower stratosphere is ~30 ppb, as shown in Figure 11b, which is consistent with that inferred from the mid-IR spectroscopy.

[49] Reactions k_{6a} and k_{10} contribute to most of the benzene formation via neutral chemistry, with a total integrated production rate of $\sim 4 \times 10^6$ cm^{-2} s^{-1}. *Vuitton et al.* [2007] suggested that the reaction between C_2H and C_4H_6 (k_5) could produce a significant amount of benzene. Because the C_4H_6 density is quite low, it appears that the column-integrated value is only 1×10^4 cm^{-2} s^{-1}, 200 times less than the other channels. The integrated benzene production rate from the electron recombination of $C_6H_7^+$ is ~3 times larger than the total production rate from neutral chemistry. Because of the general agreement with the observations, we believe that the model results strongly

Figure 11. Modeled neutral vertical profiles and comparison with observations. (a) Principal neutrals. ^{40}Ar: the stratospheric measurement was obtained by GCMS [*Niemann et al.*, 2005] and thermospheric measurements by INMS [*Yelle et al.*, 2008]. C_2H_2, C_2H_6 and C_4H_2: CIRS measurements at 15°S [*Vinatier et al.*, 2007]. (b) Aromatic species. The observed C_6H_6 mole fraction in the stratosphere was retrieved by CIRS at 15°S [*Coustenis et al.*, 2007]. Data points represent averages over 12 Titan passes of the C_6H_x density measured by INMS and presented in Table 1. Error bars include statistic uncertainties but not calibration uncertainties. "Aromatics" refers to heavy aromatic species that are not tracked in the model. (c) Principal radicals.

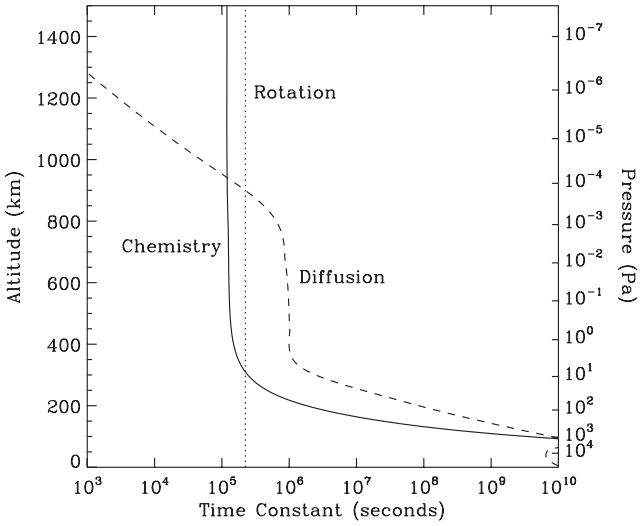

Figure 13. Modeled chemical (solid line) and diffusion (dashed line) time constants for C_6H_6. The dotted line corresponds to Titan diurnal time constant.

support the hypothesis that benzene is created by ion chemistry.

5. Discussion

[50] The results from the ion and neutral chemistry models presented in the previous sections show that the ionospheric production rate of C_6H_6 is of the right order to explain the INMS observations. These are 1D globally averaged models and do not address possible variations of C_6H_6 with latitude or local time. The strong dependence of both production and loss mechanisms on solar insulation suggests that horizontal variations could be large, whereas the results shown in Table 1 reveal that the measured variations are mild. Three-dimensional simulations that couple dynamics and chemistry are required to fully investigate horizontal variations but we can gain some insight from the timescales for chemical and transport processes.

[51] Three timescales are of interest, those for chemical processes, horizontal transport, and vertical diffusion. The chemical and diffusion time constants from our model are plotted in Figure 13. The calculated photolysis rate indicates that the chemical time constant in the upper thermosphere is 10^5 s. The diffusion time constant at 1300 km is two orders of magnitude shorter than the time constant for photolysis; it increases exponentially with decreasing altitude and becomes equal to the photolysis time constant at an altitude of 950 km. Thus chemistry is too slow to affect the altitude distribution of benzene above 950 km and it should be close to diffusive equilibrium, as calculated in the numerical models and observed by INMS.

[52] As shown in Figure 13, the diffusion time constant and chemical time constant are both within a factor of several of the diurnal time constant (equal to the length of a day divided by 2π) in the 900–1100 km region. This implies that diurnal variations are possible but should not be too extreme. The data shown in Table 1 are consistent with this. The observed variation is a factor of several. C_6H_6 is not absent on the night side, though the one measurement on the dayside (T23) implies a larger than average mole fraction. Since benzene is mostly formed on the dayside, our night side results imply that it is transported to the night side with no large loss.

[53] The situation is more complicated than simple diurnal variability however. The dynamics of Titan's upper atmosphere appear to be quite vigorous [*Müller-Wodarg et al.*, 2008] with strong meridional as well as vertical winds. The meridional winds will affect the latitudinal distribution of C_6H_6 and the vertical winds may alter both latitudinal and local time distributions, depending on the precise circulation pattern. Strong zonal winds will smooth diurnal variations. Longitude variations are also possible if some component of the circulation pattern is longitude dependent. Further observations and interpretation with 3-D simulation of dynamics and chemistry is needed to investigate these questions. At the present time, we can only say that the similarity in chemical, diffusive, and diurnal time constants is grossly consistent with the observed mild variations in abundance.

[54] *Wilson et al.* [2003] performed a study dedicated to the mechanisms for the formation of benzene in the atmosphere of Titan. They considered ion-neutral reactions and found that electron recombination of $C_6H_7^+$ controls the benzene production in the upper atmosphere. However, the production rate at 1000 km is only 10^{-2} cm^{-3} s^{-1}, one order of magnitude less than the production rate calculated here. As a consequence, the model fails to reproduce the observed benzene abundance in the thermosphere [*Wilson and Atreya*, 2003]. It is difficult to track down the discrepancy between their model and ours but the fact that the major production reaction in the ionosphere (k'_{10}) is missing in their model is probably one of the reasons. Only 13 out of the 22 reactions identified here as important for benzene formation (Table 2, Figure 8) are present in their reaction list.

[55] *Lebonnois* [2005] performed a comparative study of benzene production in Titan and Jupiter atmosphere. His model does not consider ion chemistry and the primary mechanism responsible for benzene formation is the recombination of C_3H_3 radicals (reaction k_{10} in Table 3). In the nominal simulation, the mole fraction of benzene reaches $\sim 10^{-6}$ at 1000 km, a factor of $\sim$200 higher than obtained here with neutral chemistry alone. For reaction k_{10}, *Lebonnois* [2005] adopts a value of 1.2×10^{-10} cm^3 s^{-1} for k_∞ [*Morter et al.*, 1994] and 4.4×10^{-23} cm^6 s^{-2} for k_0 at 150 K (10 times the rate for $CH_3 + CH_3$ retrieved by *McPherson et al.* [1983]). These rate constants are 3 and 80 times higher than the rate constants used here. As in our model, benzene is efficiently photodissociated into C_6H_5 radicals but in the model of *Lebonnois* [2005], the most probable fate of C_6H_5 is to form back benzene by reaction with H atoms (reaction AR7 in his Table 1). As a consequence, there is no efficient chemical loss for C_6H_5 and benzene accumulates in the atmosphere. As discussed in section 4.2, even if these reactions have yet to be studied, it is very likely that C_6H_5 does react with radicals other than H and that benzene is ultimately lost to heavier species. It follows that the high benzene abundance found by *Lebonnois* [2005] probably results from the inadequacy of the reaction list.

[56] On Earth, benzene is a major component in flames, where it appears to be associated with the formation of PAHs and soot [*Frenklach*, 2002]. Various mechanisms

involving either neutral [*Wang and Frenklach*, 1994] or ion chemistry [*Calcote and Keil*, 1990] have been proposed to explain the formation of benzene and PAHs in combustion processes. Building on these studies, *Lebonnois* [2005] and *Wilson and Atreya* [2003] suggested that PAHs were a major component of Titan's haze. However, they extrapolate kinetic data obtained at high temperature and neglect the fact that the neutral reactions involved have an activation barrier that cannot be overcome at cold temperature. As a consequence, the neutral reactions leading to PAHs in combustion processes will be inefficient on Titan. Instead, we suggest that reactions of aromatic radicals with simpler radicals (CH_3, C_2H_3, C_2H_5, etc.) along with self-reactions of aromatic radicals ($C_6H_5 + C_6H_5$) produce heavier aromatics that eventually condense and form haze that settles to the surface. We calculate a total production rate of solid aromatics of $\sim 10^{-15}$ g cm^{-2} s^{-1}. 2/3 of this mass flux is traceable to benzene produced by ion chemistry. When this process is not taken into consideration, the aromatic production rate decreases by a factor of $\sim$3, as shown in Figure 11b. Experimental studies on the reactivity of C_6H_5, C_7H_7 (benzyl) and other aromatic radicals are required to better constrain formation processes. Also, as shown in Table 4, reaction of hot benzene (k_3*) is possible at lower altitudes and some reactions could lead to the formation of more complex aromatics. Finally, considering the high density and variety of ions detected in the upper atmosphere, it is also likely that there may be other pathways in ion-neutral chemistry that could lead to aromatics.

[57] Solid benzene has been tentatively identified on Titan's surface [*Niemann et al.*, 2005; R.N. Clark, manuscript in preparation, 2008]. We calculate a benzene condensation rate of $\sim 1 \times 10^6$ cm^{-2} s^{-1}, about 1/10 of the benzene production rate. Condensation at such a rate over the age of the solar system corresponds to an average layer of only $\sim$20 cm of solid benzene on the surface of Titan at present. This condensate will be mixed with other more abundant deposits (for example, the acetylene layer is predicted to be 125 times thicker), rendering its detection by remote sensing more challenging. However, solid benzene could also be formed on the surface by heterogeneous chemistry if enough energy is available.

[58] Measurements by the CAPS Electron Spectrometer imply the existence in Titan's upper atmosphere of various negative ions ranging from $\sim$15 to $\sim$10,000 amu [*Coates et al.*, 2007]. No formation processes or attribution for these ions have been proposed to date. Dissociative attachment following low energy ($\sim$9 eV) electron impact on benzene produces $C_6H_5^-$ [*Fenzlaff and Illenberger*, 1984], which has a fairly high electron affinity (1.1 eV) [*Gunion et al.*, 1992]. More generally, dissociative electron attachment of the type:

$$\mathrm{PAH} + \mathrm{e}^-(< 15\mathrm{eV}) \rightarrow \mathrm{PAH}^{\bullet -} + \mathrm{H}$$

is an efficient process with cross sections ranging from 10^{-17} to 10^{-14} cm^2 [*Tobita et al.*, 1992]. As a consequence, $C_6H_5^-$ as well as $PAH^{\bullet -}$ are potential candidates for the negative ions observed by ELS. Complex negative ion chemistry models are necessary to further investigate this possibility.

[59] Benzene has been observed in other astronomical objects as well. It is present in the atmosphere of Jupiter [*Kim et al.*, 1985], Saturn [*Bézard et al.*, 2001] and in the proto-planetary nebula CRL 618 [*Cernicharo et al.*, 2001]. Several photochemical models have tried to reproduce the quantities of benzene observed on Jupiter and Saturn. At low-latitude, recombination of propargyl (C_3H_3) radicals is found to be responsible for most of the C_6H_6 production. In both planets, this reaction leads to abundance profiles that are $\sim$50% weaker than needed to reproduce the benzene observations [*Moses et al.*, 2000, 2005]. Under Jupiter high-latitude conditions where precipitation of energetic electrons is important, benzene is produced, as on Titan, through successive ion-neutral reactions followed by electron recombination of $C_6H_7^+$ [*Wong et al.*, 2003]. Since the benzene abundance in Jupiter's auroral regions is much higher than at low latitudes, this might indicate a possible role of meridional transport [*Lebonnois*, 2005]. Also, the models should use the two following reactions that have not been included so far:

$$\mathrm{C_2H} + \mathrm{C_4H_6} \rightarrow \mathrm{C_6H_6} + \mathrm{H}, \qquad (k_4)$$

and

$$\mathrm{C_2H_3} + \mathrm{C_4H_3} \rightarrow \mathrm{C_6H_6}, \qquad (k_{6a}).$$

[60] Benzene has also been formed in laboratory simulations of Titan's chemistry. *Imanaka and Smith* [2007] investigated the formation of complex species from a N_2/CH_4 gas mixture as a function of irradiation wavelengths from 50 nm to 150 nm. The formation of benzene is observed at wavelengths less than 80 nm, which corresponds to the photoionization threshold of N_2. This result is qualitatively consistent with the benzene formation pathways presented on Figure 8. Above 80 nm, only methane can be ionized and the formation of benzene requires the presence of species such as hydrogen cyanide (HCN) and diacetylene (C_4H_2). These are quite complex molecules that are only present at low concentration in the laboratory gas mixture, if present at all (see Figure 4 in the work of *Imanaka and Smith* [2007]). However, if N_2^+ is present, the formation of benzene only requires the presence of more simple species such as acetylene (C_2H_2) and ethylene (C_2H_4), which are readily available in the gas mixture. Modeling of the laboratory experiment would be useful in order to test this explanation in a more quantitative way.

6. Conclusions

[61] The results from analysis of the C_6H_6 time profiles combined with photochemical models of the atmosphere are:

[62] (1) The time dependence of the m/z = 77, 78 and 92 signals implies that benzene and toluene are mostly formed in the INMS chamber through $H + C_6H_5$ radicals and $CH_3 + C_6H_5$ recombination on the walls.

[63] (2) The amplitude of the m/z = 77 and 78 signals during T16 can be matched by a benzene mole fraction at 950 km of 1.3×10^{-6}.

[64] (3) The globally integrated production rate of benzene in the ionosphere, is $\sim 10^7$ cm^{-2} s^{-1}, of the same order of magnitude as the neutral production rate of $\sim 4 \times 10^6$ cm^{-2} s^{-1}. This production rate is sufficient to produce

benzene densities in Titan's upper atmosphere of the same order as that measured by INMS.

[65] (4) The total production rate of aromatics following benzene photolysis is $\sim 10^7$ cm^{-2} s^{-1} or $\sim 10^{-15}$ g cm^{-2} s^{-1} and the total benzene condensation rate is about 10% of this value. If this total deposition rate has been maintained over the age of the solar system (4.5×10^9 years), an average layer of 3 m of solid aromatic material has been deposited on the surface of Titan. However, according to the model of the history of Titan's interior from *Tobie et al.* [2006], CH_4 outgassing may have been episodic and as a consequence, the total organic production rate may be lower. This material might be at the origin of the particulates composing the dunes covering some of Titan's surface [*Lorenz et al.*, 2006].

[66] We want to emphasize that there is a need for identification of the products of $C_6H_7^+ + e^-$ (α_1) as well as for formation pathways for $C_4H_2^+$. Rates and products for the ion-neutral reactions estimated in Table 2 have to be determined. Low temperature rates for $C_2H_3 + C_6H_5$ (k_{10}) as well as low pressure and temperature rates for the other radical reactions estimated in Table 3 are also required.

[67] **Acknowledgments.** This research has been supported by the NASA grant NNG05G085G to the University of Arizona and by the NASA Cassini project through subcontract 699083KC from the Southwest Research Institute.

References

Anicich, V. G. (1993), A survey of bimolecular ion-molecule reactions for use in modeling the chemistry of planetary atmospheres, cometary comae, and interstellar clouds: 1993 supplement, *Astrophys. J. Suppl. Ser.*, *84*, 215–315, doi:10.1086/191752.

Anicich, V. G., and M. J. McEwan (1997), Ion-molecule chemistry in Titan's ionosphere, *Planet. Space Sci.*, *45*, 897–921, doi:10.1016/S0032-0633(97)00053-6.

Anicich, V. G., et al. (2003), Termolecular ion-molecule reactions in Titan's atmosphere. IV: A search made at up to 1 micron in pure hydrocarbons, *J. Am. Soc. Mass Spectrom.*, *14*, 900–915.

Anicich, V. G., et al. (2006), An ICR study of ion-molecules reactions in Titan's atmosphere: An investigation of binary hydrocarbon mixtures up to 1 micron, *J. Am. Soc. Mass Spectrom.*, *17*, 544–561.

Atkinson, D. B., and J. W. Hudgens (1999), Rate coefficients for the propargyl radical self-reaction and oxygen addition reaction measured using ultraviolet cavity ring-down spectroscopy, *J. Phys. Chem. A*, *103*, 4242–4252.

Banaszkiewicz, M., et al. (2000), A coupled model of Titan's atmosphere and ionosphere, *Icarus*, *147*, 386–404, doi:10.1006/icar.2000.6448.

Baulch, D. L., et al. (1994), Evaluated kinetic data for combustion modeling: Supplement I, *J. Phys. Chem. Ref. Data*, *23*, 847–1033.

Bézard, B., et al. (2001), Benzene on the giant planets, *Icarus*, *154*, 492–500, doi:10.1006/icar.2001.6719.

Burt, J. A., et al. (1970), Some ion-molecule reactions of H_3^+ and the proton affinity of H_2, *J. Chem. Phys.*, *52*, 6062–6075.

Calcote, H. F., and D. G. Keil (1990), The role of ions in soot formation, *Pure Appl. Chem.*, *62*, 815–824.

Cernicharo, J., et al. (2001), Infrared Space Observatory's discovery of C_4H_2, C_6H_2, and benzene in CRL 618, *Astrophys. J.*, *546*, L123–L126, doi:10.1086/318871.

Coates, A. J., et al. (2007), Discovery of heavy negative ions in Titan's ionosphere, *Geophys. Res. Lett.*, *34*, L22103, doi:10.1029/2007GL030978.

Cool, T. A., et al. (2005), Photoionization cross sections for reaction intermediates in hydrocarbon combustion, *Int. J. Mass Spectrom.*, *247*, 18–27.

Coustenis, A., et al. (2003), Titan's atmosphere from ISO mid-infrared spectroscopy, *Icarus*, *161*, 383–403, doi:10.1016/S0019-1035(02)00028-3.

Coustenis, A., et al. (2007), The composition of Titan's stratosphere from Cassini/CIRS mid-infrared spectra, *Icarus*, *189*, 35–62, doi:10.1016/j.icarus.2006.12.022.

Cravens, T. E., et al. (2005), Titan's ionosphere: Model comparisons with Cassini Ta data, *Geophys. Res. Lett.*, *32*, L12108, doi:10.1029/2005GL023249.

De Sain, J. D., and C. A. Taatjes (2003), Infrared laser absorption measurements of the kinetics of propargyl radical self-reaction and the 193 nm photolysis of propyne, *J. Phys. Chem. A*, *107*, 4843–4850.

Deakyne, C. A., et al. (1987), Proton affinities of diacetylene, cyanoacetylene, and cyanogen, *J. Chem. Phys.*, *86*, 2334–2342.

Duran, R. (1988), Is the homogeneous thermal dimerization of acetylene a free-radical chain reaction? Kinetic and thermochemical analysis, *J. Phys. Chem.*, *92*, 636–640.

Fahr, A., and A. Nayak (2000), Kinetics and products of propargyl (C_3H_3) radical self-reactions and propargyl-methyl cross-combination reactions, *Int. J. Chem. Kinet.*, *32*, 118–124.

Fahr, A., et al. (1991), Reaction rate determinations of vinyl radical reactions with vinyl, methyl, and hydrogen atoms, *J. Phys. Chem.*, *95*, 3218–3224.

Fenzlaff, H.-P., and E. Illenberger (1984), Low energy electron impact on benzene and the fluorobenzenes. Formation and dissociation of negative ions, *Int. J. Mass Spectrom.*, *59*, 185–202.

Fox, J. L., and R. V. Yelle (1997), Hydrocarbon ions in the ionosphere of Titan, *Geophys. Res. Lett.*, *24*(17), 2179–2182.

Frenklach, M. (2002), Reaction mechanism of soot formation in flames, *Phys. Chem. Chem. Phys.*, *4*, 2028–2037.

Fulchignoni, M., et al. (2005), In situ measurements of the physical characteristics of Titan's environment, *Nature*, *438*, 785–791.

Galand, M., et al. (2006), Electron temperature of Titan's sunlit ionosphere, *Geophys. Res. Lett.*, *33*, L21101, doi:10.1029/2006GL027488.

Giri, B. R., et al. (2003), The rate coefficient of the $C_3H_3 + C_3H_3$ reaction from UV absorption measurements after photolysis of dipropargyl oxalate, *Phys. Chem. Chem. Phys.*, *5*, 4641–4646.

Goulay, F., and S. R. Leone (2006), Low-temperature rate coefficients for the reaction of ethynyl radical (C_2H) with benzene, *J. Phys. Chem. A*, *110*, 1875–1880.

Gunion, R. F., et al. (1992), Ultraviolet photoelectron spectroscopy of the phenide, benzyl, and phenoxide anions, with ab initio calculations, *Int. J. Mass Spectrom.*, *117*, 601–620.

Harding, L. B., et al. (2005), Predictive theory for hydrogen atoms - Hydrocarbon radical association kinetics, *J. Phys. Chem. A*, *109*, 4646–4656.

Hedin, A. E., et al. (1973), Role of gas-surface interactions in the reduction of OGO 6 neutral particle mass spectrometer data, *J. Geophys. Res.*, *78*(22), 4651–4668.

Hirschfelder, J. O, et al. (1964), *Molecular Theory of Gases and Liquids*, Wiley, New York.

Howe, P.-T., and A. Fahr (2003), Pressure and temperature effects on product channels of the propargyl ($HC{\equiv}CCH_2$) combination reaction and the formation of the "first ring", *J. Phys. Chem. A*, *107*, 9603–9610.

Hunten, D.M., et al. (1984), Titan, in *Saturn*, edited by G. Matthews, pp. 671–759, Univ. of Arizona Press, Tucson.

Imanaka, H., and M. A. Smith (2007), Role of photoionization in the formation of complex organic molecules in Titan's upper atmosphere, *Geophys. Res. Lett.*, *34*, L02204, doi:10.1029/2006GL028317.

Kasprzak, W. T., et al. (1980), Atomic nitrogen in the upper atmosphere of Venus, *Geophys. Res. Lett.*, *7*(1), 106–108.

Kim, J. K., et al. (1977), Product distributions and rate constants for the reactions of CH_3^+, CH_4^+, $C_2H_2^+$, $C_2H_3^+$, $C_2H_4^+$, and $C_2H_6^+$ ions with CH_4, C_2H_2, C_2H_4, and C_2H_6, *J. Phys. Chem.*, *81*, 1798–1805.

Kim, S. J., et al. (1985), Infrared brightness of Jupiter 3. Spectrometry from the Voyager 1 IRIS experiment, *Icarus*, *64*, 233–248, doi:10.1016/0019-1035(85)90088-0.

Kislov, V. V., et al. (2004), Photodissociation of benzene under collision-free conditions: An ab initio/Rice-Ramsperger-Kassel-Marcus study, *J. Chem. Phys.*, *120*, 7008–7017.

Koch, E. E., and A. Otto (1972), Optical absorption of benzene vapour for photon energies from 6 eV to 35 eV, *Chem. Phys. Lett.*, *12*, 476–480.

Lavvas, P. P., et al. (2008a), Coupling photochemistry with haze formation in Titan's atmosphere. Part I: Model description, *Planet. Space Sci.*, *56*, 27–66, doi:10.1016/j.pss.2007.05.026.

Lavvas, P. P., et al. (2008b), Coupling photochemistry with haze formation in Titan's atmosphere. Part II: Results and validation with Cassini/Huygens data, *Planet. Space Sci.*, *56*, 67–99, doi:10.1016/j.pss.2007.05.027.

Lebonnois, S. (2005), Benzene and aerosol production in Titan and Jupiter's atmospheres: A sensitivity study, *Planet. Space Sci.*, *53*, 486–497, doi:10.1016/j.pss.2004.11.004.

Lee, L. C., and C. C. Chiang (1983), Fluorescence yield from photodissociation of CH_4 at 1060–1420 Å, *J. Chem. Phys.*, *78*, 688–691.

Lifshitz, C., and M. Weiss (1980), Ion-molecule reactions in aromatic systems. II. Trapped ion mass spectrometry of benzene, *Int. J. Mass Spectrom.*, *34*, 311–315.

Lorenz, R., et al. (2006), The sand seas of Titan: Cassini RADAR observations of longitudinal dunes, *Science*, *312*, 724–727.

Mackay, G. I., et al. (1980), Studies of reactions involving $C_2H_x^+$ ions with HCN using a modified selected ion flow tube, *Int. J. Mass Spectrom.*, *36*, 259–270.

Mason, E. A., and T. R. Marrero (1970), The diffusion of atoms and molecules, in *Advances in Atomic and Molecular Physics*, edited by D. R. Bates, and I. Esterman, pp. 156–226, Academic Press, New York.

McEwan, M. J., and V. G. Anicich (2007), Titan's ion chemistry: A laboratory perspective, *Mass Spec. Rev.*, *26*, 281–319.

McEwan, M. J., et al. (1999), New H and H_2 reactions with small hydrocarbon ions and their roles in benzene synthesis in dense interstellar clouds, *Astrophys. J.*, *513*, 287–293, doi:10.1086/306861.

McLain, J. L., et al. (2004), Flowing afterglow studies of the temperature dependencies for dissociative recombination of O_2^+, CH_5^+, $C_2H_5^+$, and $C_6H_7^+$ with electrons, *J. Phys. Chem. A*, *108*, 6704–6708.

McPherson, M. T., et al. (1983), The pressure and temperature dependence of the rate constant for methyl radical recombination over the temperature range 296–577 K, *Chem. Phys. Lett.*, *94*, 430–433.

Miller, J. A., and S. J. Klippenstein (2003), The recombination of propargyl radicals and other reactions on a C_6H_6 potential, *J. Phys. Chem. A*, *107*, 7783–7799.

Morter, C. L., et al. (1994), Rate constant measurement of the recombination reaction $C_3H_3 + C_3H_3$, *J. Phys. Chem.*, *98*, 7029–7035.

Moses, J. I., et al. (2000), Photochemistry of Saturn's atmosphere. I. Hydrocarbon chemistry and comparisons with ISO observations, *Icarus*, *143*, 244–298, doi:10.1006/icar.1999.6270.

Moses, J. I., et al. (2005), Photochemistry and diffusion in Jupiter's stratosphere: Constraints from ISO observations and comparisons with other giant planets, *J. Geophys. Res.*, *110*, E08001, doi:10.1029/2005JE002411.

Müller-Wodarg, I. C. F., et al. (2008), Horizontal structures and dynamics of Titan's thermosphere, *J. Geophys. Res.*, doi:10.1029/2007JE003033, in press.

Nakashima, N., and K. Yoshihara (1982), Laser photolysis of benzene. V. Formation of hot benzene, *J. Chem. Phys.*, *77*, 6040–6050.

Niemann, H. B., et al. (2005), The abundances of constituents of Titan's atmosphere from the GCMS instrument on the Huygens probe, *Nature*, *438*, 779–784.

Nizamov, B., and S. R. Leone (2004), Kinetics of C_2H reactions with hydrocarbons and nitriles in the 104–296 K temperature range, *J. Phys. Chem. A*, *108*, 1746–1752.

Pantos, E., et al. (1978), The extinction coefficient of benzene vapor in the region 4.6 to 36 eV, *J. Mol. Spectrosc.*, *72*, 36–43.

Park, J., and M. C. Lin (1997), Kinetics for the recombination of phenyl radicals, *J. Phys. Chem. A*, *101*, 14–18.

Person, J. C. (1965), Isotope effect in the photoionization efficiency for benzene, *J. Chem. Phys.*, *43*, 2553–2555.

Petrie, S., et al. (1991), The proton affinity and selected ion/molecule reactions of diacetylene, *Int. J. Mass Spectrom.*, *105*, 43–54.

Reisler, H., et al. (1980), Kinetics of free radicals generated by IR laser photolysis. IV. Intersystem crossings and reactions of $C_2(X^1\Sigma_g^+)$ and $C_2(a^3\Pi_u)$ in the gaseous phase, *J. Chem. Phys.*, *73*, 2280–2286.

Rennie, E. E., et al. (1998), A photoabsorption, photodissociation and photoelectron spectroscopy study of C_6H_6 and C_6D_6, *Chem. Phys.*, *229*, 107–123.

Richards, P. G., et al. (1994a), EUVAC: A solar EUV flux model for aeronomic calculations, *J. Geophys. Res.*, *99*(A5), 8981–8992.

Richards, P. G., et al. (1994b), Erratum: "EUVAC: A solar EUV flux model for aeronomic calculations" [J. Geophys. Res., 99, 8981–8992 (1994)], *J. Geophys. Res.*, *99*(A7), 13283–13284.

Samson, J. A. R., et al. (1987), Total and dissociative cross sections of N_2 from threshold to 107 eV, *J. Chem. Phys.*, *86*, 6128–6132.

Samson, J. A. R., et al. (1989), Ionization yields, total absorption, and dissociative photoionization cross sections of CH_4 from 110–950 Å, *J. Chem. Phys.*, *90*, 6925–6932.

Scott, G. B. I., et al. (1997), $C_mH_n^+$ reactions with H and H_2: An experimental study, *J. Phys. Chem. A*, *101*, 4973–4978.

Shafir, E. V., et al. (2003), Kinetics and products of the self-reaction of propargyl radicals, *J. Phys. Chem. A*, *107*, 8893–8903.

Stolte, W. C., et al. (1998), Dissociative photoionization cross sections of N_2 and O_2 from 100 to 800 eV, *At. Data Nucl. Data Tables*, *69*, 171–179.

Tobie, G., et al. (2006), Episodic outgassing as the origin of atmospheric methane on Titan, *Nature*, *440*, 61–64.

Tobita, S., et al. (1992), Polycyclic aromatic hydrocarbons: Negative ion formation following low energy (0–15 eV) electron impact, *Chem. Phys.*, *161*, 501–508.

Tokmakov, I. V., et al. (1999), Experimental and theoretical studies of the reaction of the phenyl radical with methane, *J. Phys. Chem. A*, *103*, 3636–3645.

Tsai, S.-T., et al. (2000), Dissociation rate of hot benzene, *J. Chem. Phys.*, *113*, 67.

Vinatier, S., et al. (2007), Vertical abundance profiles of hydrocarbons in Titan's atmosphere at 15°S and 80°N retrieved from Cassini/CIRS spectra, *Icarus*, *188*, 120–138, doi:10.1016/j.icarus.2006.10.031.

Vuitton, V., et al. (2006a), The nitrogen chemistry of Titan's upper atmosphere revealed, *Astrophys. J.*, *647*, L175–L178, doi:10.1086/507467.

Vuitton, V., et al. (2006b), Experimental and theoretical study of hydrocarbon photochemistry applied to Titan stratosphere, *Icarus*, *185*, 287–300, doi:10.1016/j.icarus.2006.06.002.

Vuitton, V., et al. (2007), Ion chemistry and N-containing molecules in Titan's upper atmosphere, *Icarus*, *191*, 722–742, doi:10.1016/j.icarus.2007.06.023.

Waite, J. H., et al. (2005), Ion neutral mass spectrometer results from the first flyby of Titan, *Science*, *308*, 982–986, doi:10.1126/science.1110652.

Waite, J. H., et al. (2007), The process of tholin formation in Titan's upper atmosphere, *Science*, *316*, 870–875, doi:10.1126/science.1139727.

Wang, H., and M. Frenklach (1994), Calculations of rate coefficients for the chemically activated reactions of acetylene with vinylic and aromatic radicals, *J. Phys. Chem.*, *98*, 11,465–11,489.

Wang, B., et al. (2003), Experimental and theoretical investigations on the methyl-methyl recombination reaction, *J. Phys. Chem. A*, *107*, 11,414–11,426.

Wilson, E. H., and S. K. Atreya (2003), Chemical sources of haze formation in Titan's atmosphere, *Planet. Space Sci.*, *51*, 1017–1033, doi:10.1016/j.pss.2003.06.003.

Wilson, E. H., and S. K. Atreya (2004), Current state of modeling the photochemistry of Titan's mutually dependent atmosphere and ionosphere, *J. Geophys. Res.*, *109*, E06002, doi:10.1029/2003JE002181.

Wilson, E. H., et al. (2003), Mechanisms for the formation of benzene in the atmosphere of Titan, *J. Geophys. Res.*, *108*(E2), 5014, doi:10.1029/2002JE001896.

Wong, A.-S., et al. (2003), Benzene and haze formation in the polar atmosphere of Jupiter, *Geophys. Res. Lett.*, *30*(8), 1447, doi:10.1029/2002GL016661.

Yelle, R. V., et al. (2008), Methane escape from Titan's atmosphere, *J. Geophys. Res.*, doi:10.1029/2007JE003031, in press.

Yung, Y. L., et al. (1984), Photochemistry of the atmosphere of Titan: Comparison between model and observations, *Astrophys. J. Suppl. Ser.*, *55*, 465–506, doi:10.1086/190963.

J. Cui, V. Vuitton, and R. V. Yelle, Lunar and Planetary Laboratory, University of Arizona, Tucson, AZ 85721, USA. (vvuitton@lpl.arizona.edu)